

Strain and Defect Engineering of Graphene for Hydrogen Storage: Atomistic Modelling

MS (Research) Thesis

By

DEEPAK KAG
(Roll number: 1904103001)



**DISCIPLINE OF MECHANICAL ENGINEERING
INDIAN INSTITUTE OF TECHNOLOGY
INDORE
JUNE 2021**

Strain and Defect Engineering of Graphene for Hydrogen Storage: Atomistic Modelling

A THESIS

*Submitted in fulfilment of the
requirements for the award of the degree
of*

Master of Science (Research)

By

**DEEPAK KAG
(Roll number: 1904103001)**



**DISCIPLINE OF MECHANICAL ENGINEERING
INDIAN INSTITUTE OF TECHNOLOGY
INDORE
JUNE 2021**



INDIAN INSTITUTE OF TECHNOLOGY INDORE

CANDIDATE'S DECLARATION

I hereby certify that the work which is being presented in the thesis entitled **Strain and Defect Engineering of Graphene for Hydrogen Storage: Atomistic Modelling** in the fulfillment of the requirements for the award of the degree of **MASTER OF SCIENCE (RESEARCH)** and submitted in the **DISCIPLINE OF MECHANICAL ENGINEERING, Indian Institute of Technology Indore**, is an authentic record of my own work carried out during the time period from July 2019 to June 2021 under the supervision of **Dr. Shailesh I. Kundalwal, Associate Professor, Indian Institute of Technology Indore**.

The matter presented in this thesis has not been submitted by me for the award of any other degree of this or any other institute.

**Signature of the student with date
(Deepak Kag)**

This is to certify that the above statement made by the candidate is correct to the best of my knowledge.

(DR. S. I. KUNDALWAL) Sept 29, 2021

Signature of the Supervisor of
MS (Research) thesis (with date)

(Dr. SHAILESH I. KUNDALWAL)

Deepak Kag has successfully given his/her MS (Research) Oral Examination held on Sept 29, 2021.

04-10-2021

Signature of Chairperson (OEB) with date

(DR. S. I. KUNDALWAL) Sept 29, 2021

Signature(s) of Thesis Supervisor(s) with date

04/10/2021

Signature of Convener, DPGC with date
date

5.10.2021

Signature of Head of Discipline with

ACKNOWLEDGEMENTS

It is a great pleasure for me to acknowledge all the people who have helped and supported me during this thesis. First and foremost, I would like to express my sincere gratitude to my advisor **Dr. Shailesh Ishwarlal Kundalwal** for the continuous support of my MS(R) study and related research, for his patience, motivation, academic support, and immense knowledge. His guidance helped me in all the time of research and writing this thesis. While working under his supervision not only enriched my academic career, but it has also nourished my inner self and significantly altered my perspective and attitude. Through my association with him, I was able to acquire, develop, and sharpen the skills and scientific methodologies that are essential for good independent research. His vast knowledge, guidance, observations, and comments greatly aided me in establishing the overall direction of the research and moving forward with in-depth investigation. For all of this, I will be eternally grateful and indebted to him.

Besides my supervisor, I would like to express my gratitude towards PSPC members **Dr. Pavan Kumar Kankar**, Department of Mechanical Engineering, **Dr. Srimanta Pakhira**, Department of Physics, **Dr. Bhupesh Kumar Lad**, Department of Mechanical Engineering, Indian Institute of Technology Indore for their insightful comments and encouragement to widen my research from various perspectives. I am grateful to **Head, DPGC Convener**, all the faculty members and staff of Department of Mechanical Engineering, **IIT Indore** for providing encouraging environment to carry out research effectively.

I would like to acknowledge **Dr. Nagesh Devidas Patil**, Department of Mechanical Engineering Indian Institute of Technology Bhilai, for his insightful ideas and comments on my work to speed up and always encourage me to do my best.

I would like to acknowledge **Prof. Neelesh Kumar Jain, Director, IIT Indore** for providing a conducive environment for research and opportunity to explore my research capabilities at IIT Indore. I am also thankful to **The Dean of Academic Affairs, The Dean of Research and Development and The Dean of Student Affairs, IIT Indore**.

I take this opportunity to thank each and every one of my friends. There have been so many of you it is impossible to name all of you. I am indebted to my seniors, lab mates and colleague researchers especially **Dr. Vijay Choyal, Dr. Kishore Shingare, Mr. Nitin Luhadiya, Dr. Vijay Kumar Choyal, Mr. Subhash Nevhal, Mr. Jagdish, Dr. Ankit Rathi, Mr. Rajnish Modanwal, Mr. Madhur Gupta, Mr. Ekansh Jain, Mr. Jayanta Sutradhar** for their cooperation and stay to make my MS(R) journey joyful and with whom I have spent so much time discussing both technical and non-technical stuff.

I take this opportunity to sincerely acknowledge the **Ministry of Human Resources and Development (MHRD)**, Government of India.

It is difficult to imagine a life without family. I would like to thank my Father **Mr. Manohar Kag**, Mother **Mrs. Kanchan Kag**, and brother **Mr. Vikash Kag**, for their constant inspiration throughout my time at IIT Indore, as well as for appreciating my work with great patience and understanding. I thank you all three for your selfless love, care, pain, and sacrifice in shaping my life. I would like to express my heartfelt

gratitude to my adorable niece **Drishiti Solanki** for bringing joy into my life and for her cuteness, which refreshed me and my family during difficult times.

Finally, I am thankful to all who directly or indirectly contributed, helped, and supported me.

-Deepak kag

Indian Institute of Technology Indore

Date: _____

Dedicated To
My Beloved Family

Abstract

Hydrogen has proven alternative fuel in terms of clean energy due to its zero-carbon emission, and the only by-product is water vapor when we use hydrogen as a fuel. Hydrogen has widespread applications, but its lack of safe and efficient onboard storage has stalled its use of in general purpose applications. The researchers are trying to find solutions for the efficient storage of hydrogen via use of different materials and techniques. One of the carbon-based nanomaterial “graphene”, a 2D material with excellent mechanical and electrical properties, has attracted a lot of attention for hydrogen storage. Graphene possesses a high specific surface area of 2630 m²/g which makes it a potential candidate to store the hydrogen via physisorption.

In this thesis, the adsorption of hydrogen molecules over the monolayer graphene via molecular dynamic (MD) simulations is studied. Interatomic interactions of carbon-carbon atoms of the graphene layer are described using the well-known AIREBO potential, while the interactions between graphene and hydrogen molecule are described using Lennard-Jones potential. In particular, the effect of strain and different defects on the hydrogen storage capability of graphene is studied. A novel method, i.e., the potential energy density method is used for the calculation of wt.% of hydrogen. A strained graphene layer was found to be more active for hydrogen storage with adsorption of 6.28 wt.% at 0.1 strain, 77 K and 10 bar. The effect of temperature and pressure on the adsorption energy and gravimetric density of graphene is also studied. Different defects in the graphene layer like monovacancy (MV), Stone Wales (SW), 5-8-5 double vacancy (DV), 555-777 DV, and 5555-6-7777 DV are considered, which usually occur during the synthesis of graphene. Among all types of defects, the MV defected graphene layer adsorbed larger amount of hydrogen with a 9.3 wt.% at 77 K and 100 bar, about 42% higher than the pristine graphene. It is also found that the critical stress and strain of defected graphene decrease appreciably compared to its pristine counterpart.

Keywords: Hydrogen storage; Molecular dynamic simulation; Graphene; Potential energy; Average adsorption energy; Strain; Vacancy defects; Physisorption; Adsorption isotherm.

Table of contents

List of figures	
List of tables	
List of abbreviations	
List of symbols	
1. Introduction and Literature Review	1-12
1.1 Hydrogen energy	1
1.2 Hydrogen storage	4
1.2.1 Methods of hydrogen storage	4
1.2.1.1 Physical storage	4
1.2.1.2 Chemical storage	5
1.2.2 Problems and motivation	6
1.3 Graphene	6
1.4 Literature on carbon-based nanostructures hydrogen storage	9
1.5 Literature on graphene sheet subjected to strain	10
1.6 Literature on defected and doped graphene	10
1.7 Scope and objective of the present work	11
1.8 Organisation of Thesis	12
2. Overview of MD Simulation	13-28
2.1 Atomistic modeling	13
2.2 Molecular dynamics (MD) simulations	14
2.2.1 Introduction	14
2.2.2 Equations of motion	15
2.2.3 Integration algorithms	16
2.2.4 Temperature control	18
2.2.5 Pressure control	20
2.2.6 Statistical ensembles	21
2.2.7 Potential fields	22
2.2.8 AIREBO potential force field	24
2.2.9 Molecular dynamics parameters	24
2.2.10 MD simulator	26
3. Effect of strain on wt.% of hydrogen stored on graphene	29-35

3.1	Introduction	29
3.2	MD modelling of graphene	30
3.2.1	Strain engineering	31
3.2.2	Gravimetric density (wt.%) calculations	32
3.3	Effect of strain	33
3.4	Conclusions	35
4	Effect of defects on wt.% of hydrogen stored on graphene	36-48
4.1	Introduction	36
4.2	MD modelling of defected sheet	37
4.3	Effect of defects	39
4.4	Conclusions	48
5	Conclusions and future scope	49-50
5.1	Major Conclusions	49
5.2	Scope for future research	50
	Appendix	51-57
	References	58-64
	List of publications from the MS(R)	65

List of Figures

Fig. No.	Caption of figure	Page No.
1.1	World total primary energy consumption.	1
1.2	Pathway to hydrogen economy.	3
1.3	Sources of hydrogen production.	3
1.4	Pathway for green hydrogen production	3
1.5	Graphene sheet.	6
1.6	sp ² hybridisation in graphene.	6
2.1	A schematic description of atomistic modeling strategies with representative length and time scales for computational simulations. Some typical nanostructures such as graphene, BN nanotube, nanosheet, and nanocomposite are shown as illustrative examples for different length and time scales.	14
2.2	Variation in the positions and velocities of atoms with the time.	17
2.3	Graphical representation of the microcanonical (NVE) ensemble, the canonical (NVT) ensemble and the isothermal-isobaric (NPT) ensemble.	22
2.4	Interatomic relative motions in molecular mechanics.	23
2.5	Equilibration of potential energy vs no. of timestep (1 fs).	25
2.6	Graphical representation of the PBCs of the middlebox. The arrows indicate the directions of the velocities of atoms. The atoms in the middlebox can interact with atoms in the neighbouring boxes without having any boundary effects.	26
2.7	The overview of LAMMPS.	28
3.1	Modelled graphene layer (black dots ●) and H ₂ molecule (blue dots ●): (a) Initial system configuration with relaxed graphene, (b) after simulation time of 1 ns, and (c) adsorbed H ₂ molecules around graphene layer.	30

3.2	Graphene layer under tension.	31
3.3	(a) Potential energy distribution of hydrogen molecules, and (b) Spatial distribution of potential energy of H ₂ molecule at 77 K and 10 bar.	32
3.4	Variation of wt.% of hydrogen adsorption on graphene with strain at 77 K and 10 bar.	34
3.5	Variation of wt.% of hydrogen adsorption on graphene and pressure with no. of timesteps.	35
4.1	Pristine and defected graphene.	38
4.2	(a) Adsorption isotherm and (b) Average adsorption energy vs pressure for pristine graphene.	39
4.3	Adsorption isotherm for MV.	41
4.4	Adsorption isotherm for SW.	41
4.5	Adsorption isotherm for 5-8-5 DV.	43
4.6	Adsorption isotherm for 555-777 DV.	43
4.7	Adsorption isotherm for 5555-6-7777 DV.	45
4.8	Isotherm curves at (a) 77 K and (b) 300 K for graphene with different vacancy defects.	45
4.9	Uniaxial tensile test in armchair direction of pristine and defected graphene.	47
4.10	Uniaxial tensile test of pristine graphene containing different concentration of defect.	47

List of Tables

Table No.	Caption of Tables	Page No.
3.1	Data related to studies performed on the strained graphene for hydrogen storage	34
4.1	The bond length of the pristine and defected sheet.	38
4.2	Comparison of critical strain and stress of pristine graphene predicted by different method.	46

List of Abbreviations

LED	Light-Emitting Diode
DST	Department of Science and Technology
HFCs	Hydrogen Fuel Cells
PV	Photovoltaic
SSA	Specific Surface Area
CVD	Chemical Vapor Deposition
HOPG	Highly Ordered Pyrolytic Graphite
AFM	Atomic Force Microscopy
STM	Scanning Tunneling Microscopy
SEM	Scanning Electron Microscope
FTIR	Fourier-Transform Infrared Spectroscopy
GO	Graphene Oxide
MD	Molecular Dynamics
DFT	Density Functional Theory
CNT	Carbon Nanotube
MV	Mono Vacancy
SW	Stone Wales
DV	Double Vacancy
LAMMPS	Large-scale Atomic/Molecular Massively Parallel Simulator
TEM	Transmission Electron Microscope
BN	Boron Nitride
REBO	Reactive Empirical Bond Order
AIREBO	Adaptive Intermolecular Reactive Empirical Bond Order
VMD	Visual Molecular Dynamics
OVITO	Open Visualization Tool

List of Symbols

F	Force
E	Potential energy
r	Position
m	Mass
a	Acceleration
v	Velocity
p	Momentum
N	Number of atoms
K_B	Boltzmann constant
T	Instantaneous temperature
t_0	Initial time
δt	Time step
N_f	Total translational degree of freedom
λ	Multiplication factor
τ	Characteristic relaxation time
T_0	Target temperature
μ	Friction factor
Q	Effective mass of thermostat
τ_T	Specified time constant for the fluctuation of temperature
P	Instantaneous pressure
V	Volume of the system
P_0	Target pressure
k	Scale factor
K_T	Isothermal compressibility
η	Nose-Hoover barostat
σ	Spacing parameter
ε	Depth parameter
\AA	Angstrom
e	Strain

Chapter 1

Introduction and Literature Review

This chapter briefly introduces hydrogen energy, production, and storage techniques. A review of literature on the storage of hydrogen over pristine graphene, graphene subjected to strain, and defected graphene. Based on the literature review, the scope of work for this thesis is identified, and the objectives of the dissertation are presented. The organization of the chapters is delineated at the end of this chapter.

1.1 Hydrogen energy

In recent years, India has connected hundreds of millions of its citizens to electricity, promoted the adoption of highly efficient LED lighting by most households, and promoted a massive expansion in renewable energy sources, led by solar power. Indian inhabitants have seen substantial improvements in their quality of life. The Covid-19 crisis, on the other hand, has hindered efforts to handle other praising issues. These include a lack of dependable electricity supply for many consumers; a continued reliance on solid biomass, primarily firewood, as a cooking fuel for approximately 660 million people; and poor air quality, which has ranked Indian cities amongst the most polluted cities in the world. India is the world's third-largest consumer of energy (Indian country status report on hydrogen and fuel cell by DST, 2020).

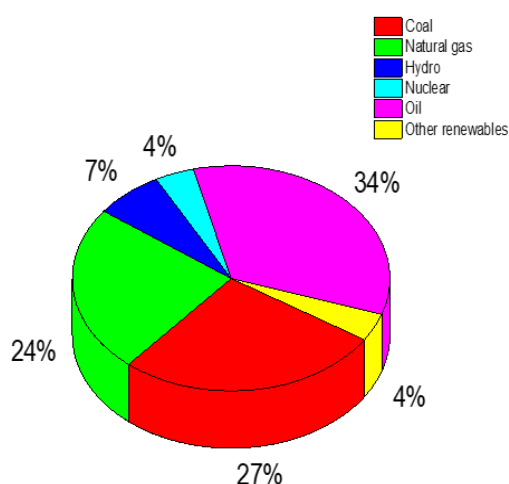


Fig. 1.1 World total primary energy consumption

More than 85 percent of energy consumption is derived from non-renewable sources, which will be depleted in the next 50 years if consumption continues at its current rate. The combustion of conventional fuels with air produces harmful gases such as CO, CO₂, SO₂, and others that harm the environment and human health (BP Statistical Review of World Energy, 2018). As a result, the replacement of fossil fuel is required, and it is critical to find an alternative fuel so that energy needs are met while also minimizing environmental pollution. Because of our ever-increasing demand for energy as well as a variety of global environmental concerns, extensive research has been conducted to find a non-carbon-emitting alternative source of energy (Durbin and Jugroot, 2013). Considering these constraints, hydrogen is a promising potential energy carrier due to its non-polluting nature, high energy content per unit mass, and zero carbon emission. More increased investment in the green energy initiative may significantly improve low-income households (Kanitkar *et al.*, 2018). The recent interest in hydrogen as an alternative fuel has resulted in a significant amount of research into the technological aspects of its production, storage, and distribution (Benard and Chahine, 2001).

Hydrogen is the lightest substance in the universe; at the same time, it is one of the abundant sources of energy and had a high energy content per unit mass of 142 MJ/kg (three times the fossil fuel) (Dante *et al.*, 2002). Hydrogen is a renewable and clean energy carrier, having water as a by-product upon consumption. Hydrogen has a widespread application, particularly in transportation (like cars, buses, and forklift trucks) and HFCs based backup power (Barrett, 2005; Houf *et al.*, 2013; Chang *et al.*, 2017). The space industry widely uses hydrogen as a fuel in rocket propulsion systems. The recent renowned interest in the use of hydrogen indicates the benefits of the use of hydrogen in the entire ecosystem. The different pathways of hydrogen economy are production, storage, transportation, and utilization. Thus, the scientific community has concluded that hydrogen has the physical and chemical advantage to be the fuel of future generations over conventional fuel (Schlapbach *et al.*, 2009). Although hydrogen is a widely available energy carrier, most of the hydrogen is present in the form of water or by forming a compound with several other components like carbon, nitrogen, etc. Therefore, we need to produce hydrogen gas to use as a fuel (Kothari *et al.*, 2006). There are three types of hydrogen-based on its sources of production, the electrolysis of water produces green hydrogen, grey hydrogen is produced by oil and coal, and blue

hydrogen is produced with the help of natural gas. Blue hydrogen can serve as a sort of steppingstone away from grey and brown hydrogen and towards a green hydrogen economy (Balat, 2009).

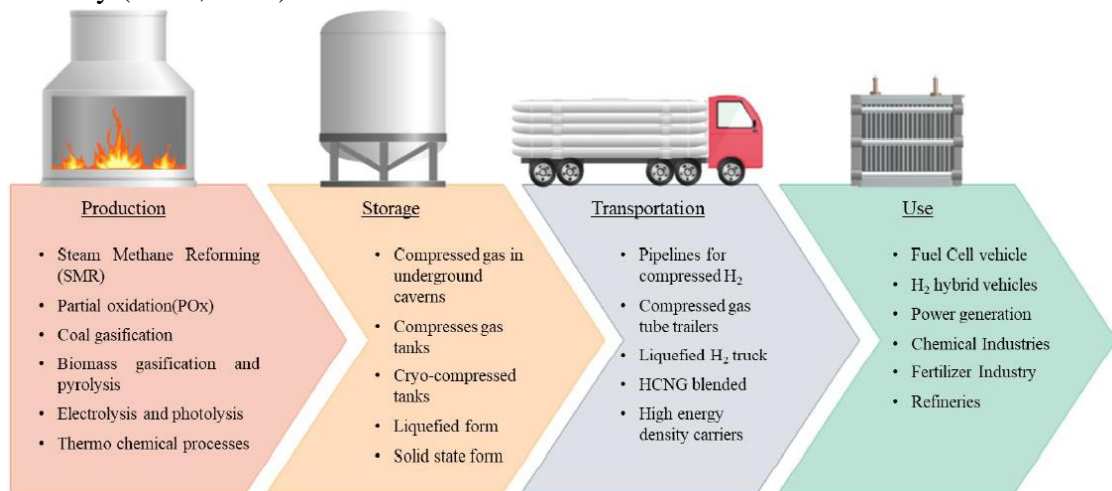


Fig. 1.2 Pathways to hydrogen economy
Indian country status report on hydrogen and fuel cell by DST, 2020

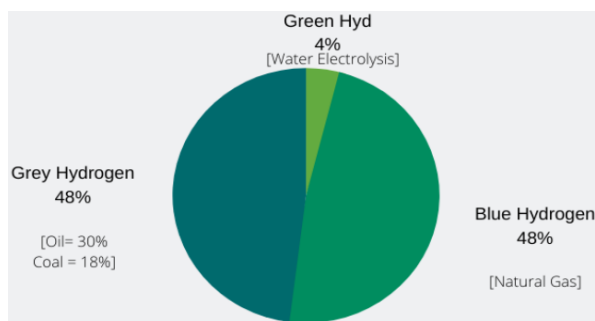


Fig. 1.3 Sources of hydrogen production
(Bartels et al., 2010)

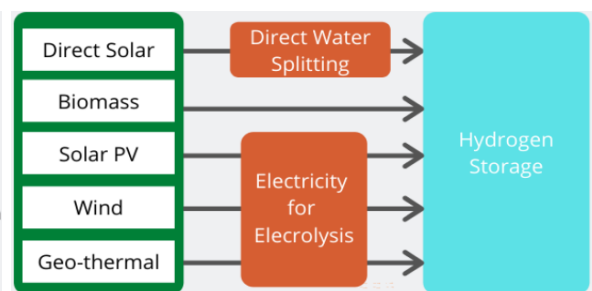


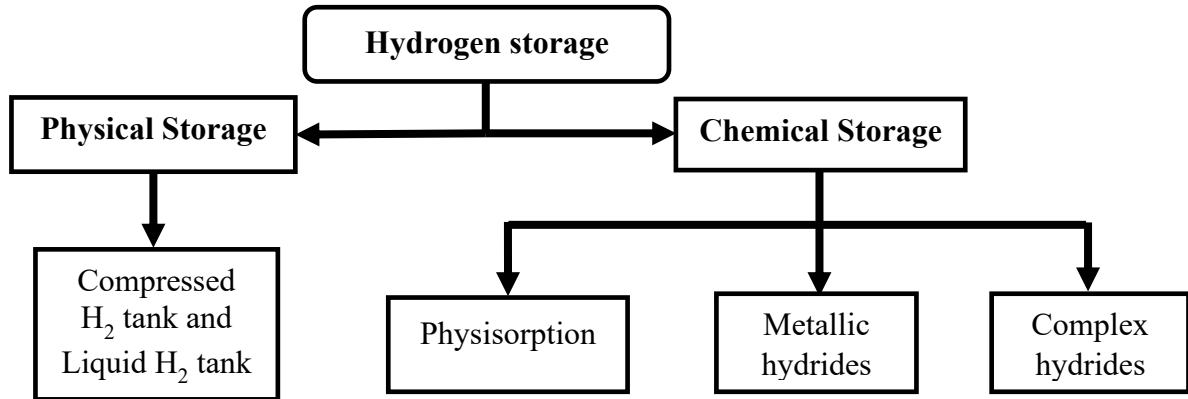
Fig. 1.4 Pathways for green hydrogen production
(Ibrahim Dincer, 2012)

Green hydrogen is produced using renewable resources and has no negative environmental impact. Direct solar, biomass, solar photovoltaic (PV), wind, and geothermal energy can all be used to produce green hydrogen. Solar energy is used directly to split water into oxygen and hydrogen molecules in the direct water splitting process. Biomass gasification is a technology pathway that converts biomass to hydrogen and other products without combustion by using a controlled process involving heat, steam, and oxygen. In electrolysis, electricity is used to generate hydrogen from water in an electrolyser (Bicakova and Straka, 2012). After the production of hydrogen, the next target is to store the hydrogen, transportation economically, and then used it as a fuel. The hydrogen can be stored in two ways physical and chemical storage. The different methods of storage of hydrogen are explained in section 1.2

1.2 Hydrogen storage

1.2.1 Methods of hydrogen storage

The following flow chart represents the different techniques for hydrogen storage (Zhou, 2005; Eberle *et al.*, 2009; Dutta, 2013).



1.2.1.1 Physical storage

- **Compressed H₂ tank:**

Hydrogen is stored as a gas in cylinders at very high pressure ranging from 400 – 700 bars. It is one of the simplest methods because of its ease of charging and discharging. The compressed hydrogen in the form of hydrogen is stored in tanks made of polymer and composite material at very high pressure that can support the mechanical forces. This approach can be suitable for vehicles. The volumetric property of the high-pressure tank must be compromised with the vehicle architecture to extend the range of the vehicle. It can be transported easily by trucks in gas cylinders or gas pipelines with a 200 – 500 bar pressures. The volumetric density can be reached up to 40 kg/m³ at a pressure of 700 bar. The problem is that the cost efficiency and energy efficiency are not that good; hence commercialization of this method for hydrogen storage is not considered.

- **Liquid H₂ tank:**

Liquid hydrogen is stored in specially insulated cryogenic tanks with provisions for cooling, heating, and venting. The density of liquid hydrogen is much higher than its gaseous form, so the volumetric efficiency is much higher than the compressed H₂ tank storage system. Liquified hydrogen tanks have a double-wall construction to keep the ultra-low temperature with thermal insulation. The problem with this type of storage system is that it requires a

large and complex system that maintains a lower temperature. So, power consumption increases, and hence storage systems become uncommercialized. Also, there is a significant temperature difference between the atmospheric temperature and stored hydrogen, so due to which the hydrogen can evaporate from the cylinder called as boil-off phenomena.

1.2.1.2 Chemical storage

- **Physisorption:**

Physisorption is also called physical adsorption, and it is a surface phenomenon. Adsorbate is getting adsorbed over the surface with adsorbent with a weak van der Waals force of attraction. Physisorption does not result in changes to the chemical bonding structure. The intermolecular attraction takes place above the critical temperature of the adsorbate and can result in the development of a monolayer and multilayer. Physisorption depends principally on the adsorption energy of the adsorbate to the substrate. Due to the weak intermolecular force of attraction, the adsorption and desorption become very easy and require a lesser amount of energy than other storage systems to desorb the hydrogen or get back hydrogen to be used as a fuel.

- **Metallic hydrides:**

The main principle of hydrogen storage in the metallic hydride storage system is that hydrogen forms a compound with the metals. First, the adsorbate is in molecular form, and then it changes into elemental form (H) and incorporates itself inside the metal lattice with the heat as output and then releases from the lattice when heat is given as input—generally, d-block element form metal hydrides.

- **Complex hydrides:**

Alanes, amides, and borohydrides are the complex hydrides used for the storage of hydrogen. The hydrogen is covalently bonded to the central atom of the complex hydrides. These materials have a high hydrogen gravimetric density. Therefore, they would seem to be a viable candidate for their application as suitable onboard hydrogen storage material. But they require a high temperature to desorb the hydrogen due to the covalent bonds.

1.2.2 Problems and motivation

From the above different available techniques for hydrogen storage, we can say that there is a problem with onboard hydrogen storage. The physical storage system looks impractical for vehicular application due to a lack of safety and volumetric constraints. In chemical storage, the metallic and complex hydrides show a potential to store the hydrogen, but there is a problem of reversibility, and the requirement of high temperature for the desorption and strength is influenced by presence of hydrogen (Chae *et al.*, 2004; Singh *et al.*, 2018). Among the available storage techniques, physisorption is a better technique for the storage of hydrogen. Physisorption is genuinely reversible, safe, portable, and more viable (Strobel, 2006). Physisorption is a surface phenomenon, which means the surfaces having a high surface area can be the potential candidate for hydrogen storage. Carbon-based nanomaterial having a very high specific area. This leads us to investigate the carbon-based nanomaterials for the storage of hydrogen (Iniguez, 2008). Among the several materials, graphene is a more viable material for hydrogen storage, and hence we are investing further in graphene.

1.3 Graphene

Graphene is one of the allotropes of carbon, having a monolayer of carbon atoms synthesized by the Manchester university group of researchers (Novoselov *et al.*, 2004). It has a hexagonal honeycomb lattice structure. Graphene exhibits excellent unique properties. It has high thermal conductivity, excellent mechanical properties (strength ~ 130 GPa), superhydrophobicity, and Young's modulus ~ 1 TPa. It is a robust material with a specific surface area (SSA) up to $2630 \text{ m}^2/\text{g}$ (Rao *et al.*, 2009). The chemical properties of carbon allow the sp^2 hybridization of the atomic orbitals (see Figure 1.6) that presents three strong in-plane (σ) bonds per atom, forming the hexagonal structure of graphene, found to be the most robust material in nature (Lee *et al.*, 2008).

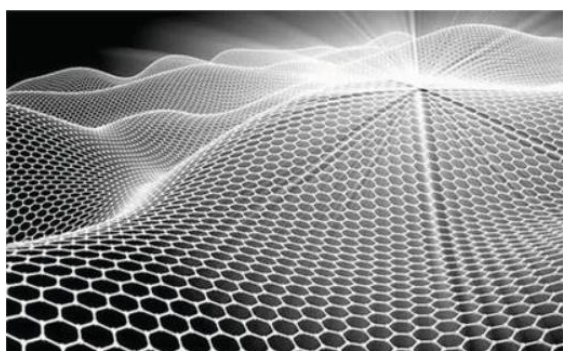


Fig. 1.5 Graphene sheet

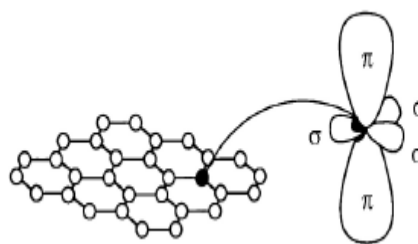
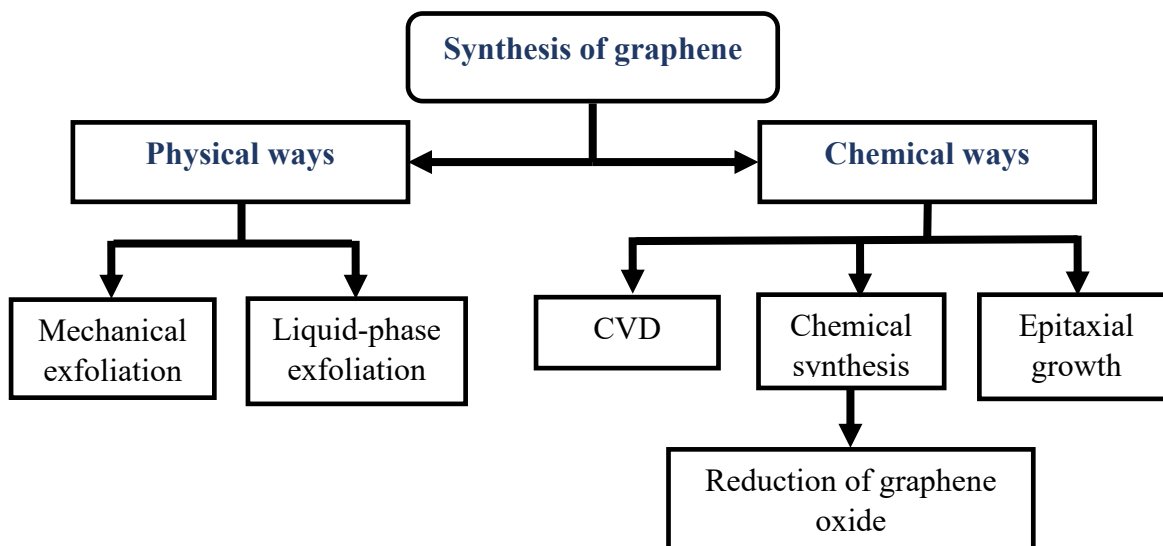


Fig. 1.6 sp^2 hybridisation in graphene

Flow chart below represents the synthesis of graphene. There are two ways for the manufacturing of graphene, physical and chemical (Choi *et al.*, 2010). Physical methods have mechanical exfoliation and liquid-phase exfoliation. Chemical methods have chemical vapor deposition (CVD), chemical synthesis, and epitaxial growth (Bhuyan *et al.*, 2016).



- **Mechanical exfoliation**

It is the first recognized method for the synthesis of graphene. This is a top-down technique in nanotechnology. Graphene sheets of different thickness can indeed be obtained through mechanical exfoliation or by peeling off layers from graphitic materials such as highly ordered pyrolytic graphite (HOPG), single-crystal, and natural graphite. Exfoliation is the reverse of stacking, can be done by using a variety of agents like scotch tape, ultrasonication, AFM tips, etc. It is one of the cheapest method to get the monolayer of graphene. Synthesized graphene can be characterized by Raman spectroscopy, STM, AFM, SEM, and FTIR.

- **Liquid-phase exfoliation**

Liquid-phase exfoliation is the principal method to produce 2D materials such as graphene in large quantities with a good balance between quality and cost. The fragmentation and exfoliation mechanisms involved have usually been simply attributed to the force induced by ultrasound and the interaction with the solvent molecules. First sonication leads to the fragmentation of large flakes

and after the second sonication, the final stage is the exfoliation to separate the different layered graphene.

- **Chemical vapor deposition (CVD)**

Chemical vapor deposition is one of the best methods for the mass production of graphene. CVD comprises a chemical reaction in which process molecules are heated and changed to a gaseous state called as precursor. In this CVD process, a substrate is diffused on thermally disintegrated precursors at high temperatures. Then, the precursors are deposited on the surface of the substrate. For the growth of graphene through CVD, mainly used the Cu and Ni substrate.

- **Chemical synthesis**

Chemical synthesis is one of the conventional methods to produce graphene in large quantities. Graphene oxide (GO) is readily prepared by the Hummers method involving the oxidation of graphite with strong oxidizing agents such as KMnO_4 and NaNO_3 in H_2SO_4 . Then exfoliation is performed to obtain the fragmented GO and then chemical reduction of GO to obtain graphene samples.

- **Epitaxial growth**

Epitaxial growth on a single crystalline silicon carbide (SiC) surface is one of the most praised graphene synthesis methods. When the deposition of the single crystalline film on a single crystalline substrate produces epitaxial film, and the process is known as epitaxial growth. In this method, the SiC substrate is used, and after thermal treatment in a vacuum at a temperature of $1200 - 1300$ °C, Si evaporates from its surface and gets the layer of carbon atoms over the surface.

Graphene has a widespread application (Chung *et al.*, 2012; Perreault *et al.*, 2015) like:

- Biomedicals - for the targeted drug delivery, smart implants.
- Composite and coating – to strengthen and make the flexible composite.
- Electronics – semiconductors, bendable phones, faster transistors.
- Energy – due to its high SSA, can be used to store hydrogen, used in electric cars to reduce charging time.
- Sensors – ultra-sensitive sensors.

- Membranes – for cleaning water.

1.4 Literature on carbon-based nanostructures hydrogen storage

Synthesized graphene may consist of a monolayer, a single layer of carbon atoms, a bi-layer, and a few layers consisting of 3 to 10 layers. Various carbon-based nanomaterials are investigated for hydrogen's physisorption, and a lot of work has been done so far. Ci et al. (2002) experimentally found that the annealed CNT at the temperature range of 1700-2200 °C can store the hydrogen up to 3.98 wt.%. Hirscher and Panella (2005) experimentally found that the carbon nanostructure has a high SSA and can store the hydrogen up to 4.5 wt.% at 77K. Jin et al. (2007) experimentally investigated the microporous activated carbons with a SSA of 2800 m²/g and achieved the maximum hydrogen adsorption of 1 wt.% at room temperature. Subsequently, Braga et al. (2007) studied the carbon nanoscrolls at a lower temperature of 77 K; at this temperature, hydrogen gets adsorbed. At a higher temperature of 300 K, hydrogen gets desorbed using atomistic molecular dynamics. Armandi et al. (2008) experimentally investigated the hydrogen adsorption at porous graphene at different temperatures with a maximum hydrogen uptake of 2 wt.%, and pores play a significant role in physisorption. Ma et al. (2009) experimentally studied the hydrogen adsorption behaviour of graphene sheets in powder form at 77 K and 100 KPa. They found that the specific surface area and binding of hydrogen are responsible for the wt.% of H₂. Wu et al. (2012) studied pillared graphene using the MD simulations. They found that low temperature and high pressure with large interlayer distances maximize hydrogen storage and nullify the edge effect. Srinivasan et al. (2010) experimentally fabricated the graphene powder by reducing exfoliated graphite oxide and observed a hydrogen wt.% of 1.2 and 0.1 at 77 K and 298 K, respectively. Cooper et al. (2012) studied the hydrogen adsorption on single-layer graphene using the newly developed van der Waal density functional. They concluded that the molecular hydrogen, closer to the surface, has a more significant interaction with graphene. Zheng et al. (2013) investigated the adsorption equilibrium of hydrogen on graphene sheet experimentally at 77 K – 293.15 K. They found that hydrogen molecules strongly interact with the graphene sheet and have a high specific surface area that leads to higher adsorption of hydrogen.

1.5 Literature on graphene sheet subjected to strain

Graphene has a very high SSA, due to which it is the potential candidate for the storage of hydrogen via physisorption. From the above literature, researchers have investigated graphene for the storage of hydrogen. They modified graphene's surface, making it active by providing the strain to it. Zhou et al. (2010) studied the effect of strain on the hydrogen storage capability of metal decorated graphene. Their results revealed that strain prevents the metal from clustering and increases the hydrogen uptake. Xue and Xu (2010) studied the effect of biaxial strain up to 10 % using the first principle on graphene. They concluded that structurally deformed graphene has more potential to store hydrogen as compared to pristine. Surya et al. (2012) observed that the monolayer of graphene becomes chemically active by physical modification, and the introduction of strain is a non-destructive technique. The study highlights the interplay between the induced strain and the adsorption of chemical species. Hussain et al. (2012) investigated the effect of biaxial strain on the Li doped graphene sheet with first-principles density functional theory. Their results reveal that the strain increases lithium stability and enhances the storage capacity of hydrogen storage. Deng et al. (2018) studied the effect of strain engineering on 2D nanomaterials. They revealed that strain modifies the atomic structure, lattice vibration, chemical activity, thermal conductivity, and mechanical properties.

1.6 Literature on defected and doped graphene

During the synthesis of graphene, a change in the cooling rate results in the graphene sheet with different types of vacancy defects. Defected graphene shows altered properties and has a more significant potential to capture more hydrogen. Park et al. (2010) studied the boron substituted Li decorated graphene sheet using the density functional theory (DFT). Their results revealed that the boron substitution enhances lithium-decorated sheets for hydrogen adsorption and results in high hydrogen storage. Wang et al. (2011) experimentally investigated the Ni-B doped graphene via the chemical reduction method. They obtained the maximum hydrogen storage uptake up to 2.81 wt.% at 77 K temperature. Sen et al. (2013) studied the effect of different double vacancy (DV) defected graphene sheets for hydrogen storage using the DFT calculations and MD simulations. Their results reveal that the defected sheet is well suited for hydrogen storage compared to pristine with lower adsorption energy and has excellent stability. Kim et al. (2014) studied the lithium decorated defected

graphene for hydrogen storage using the DFT. They observed that the SW defected graphene attracted more Li atoms and showed greater potential to store the hydrogen. Subsequently, Yadav et al. (2014) investigated the effect of different types of vacancy defects on graphene for hydrogen storage using the DFT. Their results revealed that the defected graphene sheet has lower adsorption energy and binds hydrogen with a maximum gravimetric density of 7.02%. Seenithurai et al. (2014) studied the Li decorated double carbon vacancy defect graphene (DVG) for hydrogen storage application using the DFT calculations. They found that lithium atoms' decoration is enhanced with defected graphene and can be helpful in reversible storage applications with 7.26 wt.%. Ao et al. (2014) investigated the adsorption of hydrogen molecules over porous graphene decorated with Al using DFT calculations. They found that the Al enhances the interaction of H₂ molecules towards porous graphene, and gravimetric density can reach up to 10.5 wt.%. Nagar et al. (2017) reviewed the H₂ storage capabilities of chemically modified graphene-based materials. They concluded that combining structural/surface modifications could create a pathway to elevate the H₂ storage capacity. Arhilaran et al. (2017) experimentally investigated the nitrogen-doped graphene and found that the nitrogen-doped graphene material can hold up to 1.5wt.% of H₂ at room temperature and 90 bar pressure. Shiraz and Tavakoli (2017) reviewed the graphene-based material for the storage of hydrogen. They have found that the porous, activated, and defected graphene material can be a potential candidate for hydrogen storage. Das et al. (2018) experimentally studied the N-doped porous carbon and found that the pore size has been correlated with hydrogen storage. A large number of pores with a lower pore diameter is preferable to increase hydrogen storage capacity. Tiwari and Sharma (2019) numerically investigated the metal hydrides for hydrogen storage and found that it is possible to integrate a low-cost sensible heat-storage system, and it is helpful for high-temperature.

1.7 Scope and objective of the present work

A literature survey indicates that numerous experimental and first-principle studies on carbon nanostructures (CNT, graphene, etc.) have been performed for hydrogen storage. Some of the studies were performed on graphene using MD simulations (Wu *et al.*, 2012; Simon *et al.*, 2010; Borodin *et al.*, 2011; Ansari *et al.*, 2012; Sen *et al.*, 2013; Alian *et al.*, 2017). To the best of our knowledge, no single study reports the effect of strain and vacancy defects on the hydrogen adsorption on the large-

area graphene layer using the MD simulations. This has inspired us to conduct the present work. The work stated in this thesis is based on the modification of graphene by providing the strain and different structural defects like monovacancy (MV), Stone Wales (SW), and double vacancy (DV), and analyse the H₂ adsorption and desorption capability. We also examine the effect of pressure and temperature on adsorption and desorption phenomena using the MD simulations. Additionally, we widen our research scope beyond this and find the change in mechanical strength when we created different defects in the graphene layer. As a strikingly novel research goal, it is intended to accomplish the tasks of the following objectives:

- Study the graphene sheet subjected to the strain along the armchair direction, determine its energetic stability, and its effect on hydrogen storage via MD simulations.
- Study the effect of different types of vacancy defects on hydrogen storage considering the different temperature and pressure.
- Investigate the effect of vacancy defects on the strength of graphene sheet via MD simulations.

1.8 Organisation of Thesis

The remaining part of the thesis is organized as follow:

- Chapter 2 deals with the overview of MD simulations, potential used, thermodynamic ensembles, boundary conditions, MD parameters, and MD simulator (LAMMPS).
- Chapter 3 presents the sheet subjected to varied strain, equilibration of the system, and wt.% calculation at particular strain at specified temperature and pressure.
- Chapter 4 deals with the effect of different types of vacancy defects on hydrogen storage and which defect adsorbs the large amount of hydrogen at different temperatures and pressures.
- Chapter 5 summarizes the major conclusions drawn from the research work presented in the thesis and the future scope of research on graphene. The references are alphabetically listed at the end of the thesis.

Chapter 2

Overview of MD simulations

This chapter outlines the overview of the MD simulations, pressure and temperature control, thermodynamic ensemble, potential field, MD parameters, and MD simulator (LAMMPS). In addition, steps taken during the simulation (Modelling of graphene, Input script, obtaining the trajectories, and finally analyzing the output) are also discussed.

2.1 Atomistic modeling

Nanomechanics is the new branch of mechanics associated with the study and characterization of behavior/properties of nanostructures in response to different types of loading conditions. Any structure with a dimension less than 100 nm (10^{-7} m) is considered a nanostructure. A thorough understanding of the physics of nanomaterials is required for the design and development of their structures. This is usually achieved by using nanomechanical experiments or theoretical models. For instance, TEM, SEM, AFM, nanoindenter, etc., are widely used to characterize nanomaterials experimentally. However, conducting experiments at the nanoscale level is very expensive, complicated, and time-consuming due to the involvement of atomistic parameters. Therefore, atomistic modelling plays a vital role in nanomechanics.

Over the past three decades, there has been a rapid advancement in research activity on nanostructured materials, with the long-term promise to tailor design material properties at the nanoscale level. In such noble efforts, computations are playing an essential role in complementing experiments. Atomistic modelling-based techniques use modern computing power to include every atom of the system under consideration in its modelling as interacting particles are the foundation of materials science. Virtual computational experiments can significantly reduce the cost and accelerate the time scales of understanding and developing new materials without synthesizing them. A schematic illustration of typical atomistic modelling strategies is shown in Fig. 2.1.

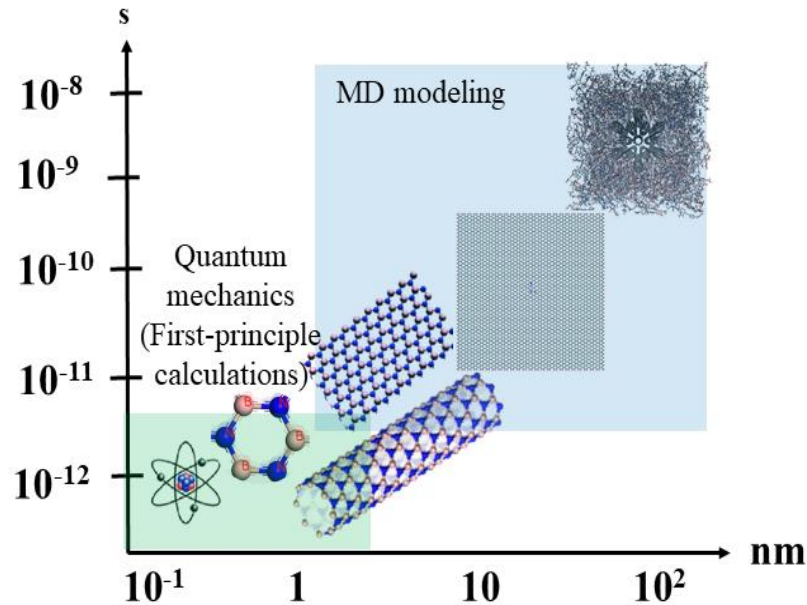


Fig. 2.1 A schematic description of atomistic modeling strategies with representative length and time scales for computational simulations. Some typical nanostructures such as graphene, BN nanotube, nanosheet, and nanocomposite are shown as illustrative examples for different length and time scales.

2.2 Molecular dynamics (MD) simulations

Molecular dynamics (MD) technique is one of the most efficient and attractive atomistic modelling method (Rapaport, 1996). In MD technique, the atom is assumed as an interacting classical particle, and the interatomic interactions between the atoms are described using molecular mechanics force fields.

2.2.1 Introduction

MD simulation is one of the most widely used techniques in the study of nanostructures. It is a nanomechanics based computer simulation technique in which the time evaluation of a set of interatomic interactions of atoms is followed by integrating their equations of motion. The time dependent integration is done by solving the classical Newton's equations of motion numerically. The interatomic interactions between the atoms of nanostructure are described by molecular mechanics potential fields. MD simulations allow gaining insight into nanostructure under the specific condition that is impossible to study experimentally. This serves as a complement to

conventional experiments with cheaper and faster outputs. MD simulations have an advantage over classical models as it provides a route to dynamical properties of the molecular system such as time-dependent responses to perturbations, transport coefficients, thermo-mechanical properties, rheological properties, and spectra, and many more characteristics of the system. Therefore, the MD simulations were performed in the current study using open-source software, Large-scale Atomic/Molecular Massively Parallel Simulator (LAMMPS) (Plimpton, 1995).

2.2.2 Equations of motion

MD simulation is divided into two steps. The first step involves the determination of interatomic interacting forces of atoms using molecular mechanics-based potential fields. The second step involves the tracing of trajectories of movements of atoms by integrating the equations of motion. The interatomic forces between the atoms are determined from the gradient of a molecular mechanic's potential field during the simulations, and the force acting on an atom α is given by (Rapaport, 1996):

$$F_{\alpha} = - \frac{\partial E_{\alpha}}{\partial r_{\alpha}} \quad (2.1)$$

where F_{α} is the force exerted, E_{α} is the potential energy, and r_{α} is the position of an atom α . The potential energy of atoms is obtained from the molecular mechanic's potential field, and an appropriate potential field to simulate the graphene is discussed in section 2.2.8. The force acting on each atom is known, and using Newton's second law, the acceleration of each atom can be obtained by:

$$F_{\alpha} = m_{\alpha} \frac{d^2 r_{\alpha}}{dt^2} = \frac{dv}{dt} = m_{\alpha} a_{\alpha} \quad (2.2)$$

where m_{α} and a_{α} are the mass and acceleration of atom α , respectively.

A system of atoms can move under accelerations for a period called time step. The velocity of atom α at each time step can be obtained and then using it, the position of atom α can be calculated. Therefore, to calculate the trajectory of atoms, only the initial positions of atoms, initial distribution of velocities, and accelerations are required, and these are obtained by the gradient of potential energy function. The initial distribution of velocities of the atoms of the system is usually determined from a random distribution with the

magnitudes conforming to the required temperature and corrected, so there is no overall momentum (p) in the atoms of the systems, i.e.,

$$p = \sum_{\alpha=1}^N m_{\alpha} v_{\alpha} = 0 \quad (2.3)$$

The velocities v_{α} are often chosen randomly from a Maxwell-Boltzmann or Gaussian distribution at a given temperature, which provides the probability that an atom α has a velocity v_x in the x direction at a temperature T .

$$p(v_{\alpha x}) = \left(\frac{m_{\alpha}}{2\pi K_B T} \right)^{1/2} \exp \left[-\frac{1}{2} \frac{m_{\alpha} v_{\alpha x}^2}{K_B T} \right] \quad (2.4)$$

$$T = \frac{1}{3N} \sum_{\alpha=1}^N \frac{|p_{\alpha}|^2}{2m_{\alpha}} \quad (2.5)$$

where N is the number of atoms in the system and k_B is Boltzmann's constant.

2.2.3 Integration algorithms

The potential energy of interatomic interactions of atoms is the function of their positions in the system. Numerous numerical algorithms such as leap-frog algorithm (Hockney, 1970), velocity Verlet algorithm (Swope *et al.*, 1982) etc. have been developed for integrating the equations of motion. MD is usually applied to a large-scale atomistic model, and the energy evaluation is time-consuming, and memory requirement is also large. To generate the correct statistical ensembles, energy conservation is required.

Thus, the basic criteria for the right integrator for simulations are as follows:

- It should be fast, ideally requiring only one energy evaluation per timestep.
- It should require less computer memory.
- It should permit the use of a relatively long timestep.
- It must show functional conservation of energy.

In all the integration algorithms, the positions, velocities, and accelerations of atoms can be approximated by a Taylor series expansion (Rapaport, 2011).

$$r(t_0 + \delta t) = r(t_0) + v(t_0)\delta t + \frac{1}{2}a(t_0)\delta t^2 + \dots \quad (2.6)$$

$$v(t_0 + \delta t) = v(t_0) + a(t_0)\delta t + \frac{1}{2}b(t_0)\delta t^2 + \dots \quad (2.7)$$

$$a(t_0 + \delta t) = a(t_0) + b(t_0)\delta t + \dots \quad (2.8)$$

where r , v , and a are the positions, velocity, and acceleration of an atom, respectively, t_0 is the initial time, and δt is the time step. The change in r and v with δt are graphically represented in Fig. 2.2.

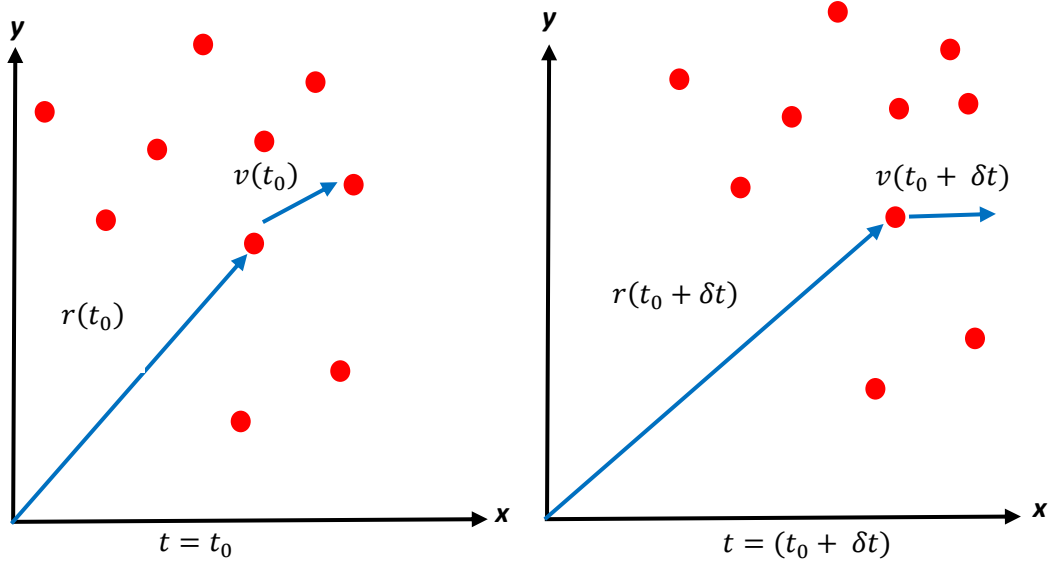


Fig. 2.2 Variation in the positions and velocities of atoms with the time.

The following numerical algorithms have been developed for integrating the equations of motion in the literature:

Leap-Frog Algorithm (Rapaport, 1996): The velocities at the time $t + \frac{1}{2}\delta t$ is first calculated and then the position r is obtained at time $t + \delta t$ using the obtained velocities in first step. The advantage of this algorithm is that the velocities are explicitly calculated; however, the disadvantage is that they are not calculated at the same time as the positions.

$$r(t_0 + \delta t) = r(t_0) + v\left(t_0 + \frac{1}{2}\delta t\right)\delta t \quad (2.9)$$

$$v\left(t_0 + \frac{1}{2}\delta t\right) = v\left(t_0 - \frac{1}{2}\delta t\right) + a(t_0)\delta t \quad (2.10)$$

The velocities at time t can be approximated by:

$$v(t_0) = \frac{1}{2} \left[v \left(t_0 - \frac{1}{2} \delta t \right) + v \left(t_0 + \frac{1}{2} \delta t \right) \right] \quad (2.11)$$

Beeman's Algorithm (Rapaport 1996): This algorithm is closely related to the Verlet algorithm. According to the algorithm the respective position and velocity can be described by,

$$r(t_0 + \delta t) = r(t_0) + v(t_0)\delta t + \frac{2}{3}a(t_0)\delta t^2 - \frac{1}{6}a(t_0 - \delta t)\delta t^2 \quad (2.12)$$

$$v(t_0 + \delta t) = v(t_0) + v(t_0)\delta t + \frac{1}{3}a(t_0)\delta t + \frac{5}{6}a(t_0)\delta t - \frac{1}{6}a(t_0 - \delta t)\delta t^2 \quad (2.13)$$

The advantage of this algorithm is that it provides a more accurate expression for the velocities and better energy conservation. The disadvantage is that the more complex expressions make the calculations more expensive.

Velocity Verlet Algorithm (Swope *et al.*, 1982): The new positions and velocities of atoms are obtained by using a numerical integration method. According to the velocity Verlet method, position and velocity can be obtained by,

$$v \left(t_0 + \frac{\delta t}{2} \right) = v(t_0) + a(t_0) \frac{\delta t}{2} \quad (2.14)$$

$$r(t_0 + \delta t) = r(t_0) + v \left(t_0 + \frac{\delta t}{2} \right) \delta t \quad (2.15)$$

$$v(t_0 + \delta t) = v \left(t_0 + \frac{\delta t}{2} \right) + a(t_0) \delta t \quad (2.16)$$

The velocity Verlet algorithm is widely used in MD simulation due to the less computer memory requirement as only one set of positions, velocities, and forces need to calculate at one time.

During MD simulation, controlling temperature and pressure is necessary in order to simulate the real system. The temperature control is achieved by modifying the velocities of atoms, while pressure is controlled by adjusting the size of the simulation box. A review of commonly used techniques to control temperature and pressure is given below.

2.2.4 Temperature control

The temperature is a state that defines the thermodynamic state of the system. The temperature of a system is the average of kinetic energies of all the atoms, which is calculated from the atomic velocities and can be given as (Rapaport, 1996):

$$T = \frac{1}{k_B N_f} \sum_{i,\alpha} m^\alpha (v_i^\alpha)^2 \quad (2.17)$$

where k_B is Boltzmann's constant, N_f is the total translational degree of freedom of the system, m^α is the mass of atom α , and v_i^α is the velocity of atom α in i direction.

During the simulation, it is not possible to keep temperature constant due to the fluctuations of velocities of atoms of the system. Hence, the average value of temperature can be maintained during the MD simulation. According to Eq. (2.17), the system temperature depends on the velocities of atoms. Therefore, by scaling the velocities of atoms, the temperature can be controlled, which is usually accomplished by a thermostat. The most commonly used thermostats are Anderson, Berendsen, and Nose-Hoover.

Anderson thermostat (Andersen, 1980): This is the most straightforward thermostat, and, in this method, the velocity of a random particle is replaced by a value chosen from the Maxwell-Boltzmann distribution for a given temperature. Anderson's thermostat is computationally expensive.

Berendsen thermostat (Berendsen *et al.*, 1984): This is the most commonly used thermostat due to its simplicity and easy implementation. To maintain the constant temperature during the simulation, the system is coupled to an external heat bath source with fixed temperature T_0 . The velocities of atoms are scaled at each time state such that the change in the rate of temperature is proportional to the difference in temperature:

$$\frac{dT(t)}{dt} = \frac{1}{\tau}(T - T(t)) \quad (2.18)$$

This method provides an exponential decay of the system towards the target temperature using a factor λ :

$$\lambda = \left[1 - \frac{\delta t}{\tau} \left(\frac{T - T_0}{T}\right)\right]^{\frac{1}{2}} \quad (2.19)$$

where τ is the characteristic relaxation time, δt is the timestep size, T is the instantaneous temperature, and T_0 is the target temperature. This method maintains a constant temperature with good approximation, and the temperature can be controlled by changing τ and adjusting T_0 .

Nosé-Hoover thermostat (Nosé, 1984): This is a method for performing constant-temperature dynamics that produces true canonical ensembles in both momentum and coordinate spaces. This method was used in this study because it is one of the best-considered thermostats among all the thermostats (Hünenberger, 2005). This thermostat uses a friction factor (μ) to alter the equations of motion, as follows:

$$\frac{d\mu(t)}{dt} = \frac{k_B N_f}{Q} (T(t) - T_0) \quad (2.20)$$

where Q is the effective mass of the thermostat:

$$Q = k_B N_f T(t) \tau_T^2 \quad (2.21)$$

where τ_T is the specified time constant for the fluctuations of temperature. To achieve the smooth temperature transition, the time constant value is usually considered in the order of hundred-time steps. The modified equation of motion is defined by,

$$a = \frac{f(t)}{m} - \mu(t)v(t) \quad (2.22)$$

2.2.5 Pressure control

The pressure is a basic thermodynamic variable that provides the state of the system of atoms and is defined as:

$$P_{ij}^V = \frac{1}{V} \sum_{\alpha} \left[\sum_{\beta=1}^N (r_i^{\beta} - r_i^{\alpha}) f_j^{\alpha\beta} + m^{\alpha} v_i^{\alpha} v_j^{\alpha} \right] \quad (2.23)$$

where V is the volume of the system, β is assigned a number to neighbor atoms that pass from one to the number of neighboring atoms (N), and r_i^{α} and r_i^{β} are the positions of atoms α and β along the direction i , respectively. Term $f_j^{\alpha\beta}$ is the force along the j direction on atom α due to atom β , and v^{α} and m^{α} are the velocity and mass of atom α , respectively.

During the simulation, the pressure of the system of atoms can be adjusted by changing the dimension of the simulation box. This can be achieved using the barostat during the simulations, and the most commonly used barostats are Berendsen (Berendsen *et al.*, 1984) and Nose-Hoover barostat (Martyna *et al.*, 1994).

Berendsen barostat maintains the pressure of a system at a target value. Berendsen method couples the system to a pressure bath. At each time step, size of the simulation box and the coordinates of atoms are rescaled. At each step, x , y , and z coordinates of each atom are scaled by the factor, μ :

$$\mu = \left[1 - \frac{\delta t}{\tau} \gamma [P - P_0] \right]^{\frac{1}{3}} \quad (2.24)$$

where P is the instantaneous pressure, P_0 is the target pressure, and δt is the time step. The same factor scales the cartesian components of the unit cell vectors. Berendsen's method is less reliable compared to the Nose-Hoover method (Hünenberger, 2005).

Nose-Hoover barostat (η) is defined as

$$\frac{d\eta}{dt} = \frac{1}{k_B N_f T_0 \tau_p^2} V(t) (P(t) - P_0) \quad (2.25)$$

where τ_p is the specified time constant for pressure fluctuations, and its value usually on the order of thousands of time steps to achieve a smooth pressure fluctuation. The controlled volume of the system is determined by using the following relation:

$$\frac{dV(t)}{dt} = [3\eta(t)]V(t) \quad (2.26)$$

2.2.6 Statistical ensembles

The whole universe is governed by the thermodynamics laws through the transfer of energy between matter. This is attributed to the change in the total energy of the system. This process is very complex to consider directly; therefore, several parts of the universe, i.e., the system, is considered separately, and it can be described using an ensemble. An ensemble is a collection of all possible states of the real systems that have identical thermodynamic or macroscopic states but have different microscopic states. The commonly used ensembles are (i) constant N , V , and E (NVE) or microcanonical ensemble, (ii) constant N , V , and T (NVT) or canonical ensemble, and (iii) constant N , P , and T (NPT) or isothermal-isobaric ensemble. The N , V , E , T , and P denote the number of atoms, volume, energy, temperature, and pressure of the system of atoms, respectively. The graphical representations of ensembles are shown in Fig. 2.3.

Microcanonical ensemble (NVE) is derived from Newton's law of motion without any pressure and temperature control (Rapaport, 1996). The energy of the system is conserved during the simulations. The NVE ensemble is a statistical ensemble that keeps

the constant specified total energy of all the possible states of mechanical systems. The system's energy, volume, composition, and shape are kept constant in all possible states of the system.

Canonical ensemble (NVT) can be obtained by maintaining the constant thermodynamic temperature, total volume, and the number of particles in the system. (Rapaport, 1996). The NVT ensemble is a statistical mechanics ensemble that denotes the possible states of the mechanical system in the thermal equilibrium of heat bath at finite temperature. The system allows only to exchange the energy from the heat bath, and the energy is no longer constant.

Isothermal-Isobaric ensemble (NPT) allows the control of both the pressure and temperature of the system (Rapaport, 1996). The NPT ensemble is a statistical mechanical ensemble that maintains a constant total number of particles, pressure, and temperature. NPT can also be used during equilibration to obtain the desired pressure and temperature before changing to the constant-energy and constant-volume ensembles.

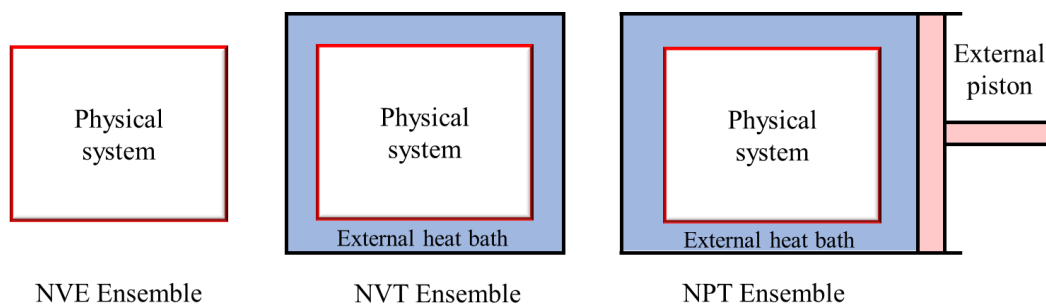


Fig. 2.3 Graphical representation of the microcanonical (NVE) ensemble, the canonical (NVT) ensemble and the isothermal-isobaric (NPT) ensemble (Gale et al., 2012).

2.2.7 Potential fields

The potential field is a mathematical description of the potential energy of a system of interacting atoms. The empirical relation of potential energy parameters in potential fields is derived from high-level quantum mechanical calculations and experimental studies. To simulate the different molecular systems required a unique potential field. The general form of a potential field as a function of energy and can be defined as

$$E_{total} = E_{covalent} + E_{non\ covalent} \quad (2.27)$$

where E_{total} , $E_{covalent}$, and $E_{non\ covalent}$ are the total energy, covalent energy, and non-covalent energy, respectively, and interatomic relative motions in molecular

mechanics depict in Fig. 2.4. The components of covalent and noncovalent energies can be expressed as

$$E_{covalent} = E_{bond} + E_{angle} + E_{dihedral} + E_{out-of-plane} \quad (2.28)$$

$$E_{non\ covalent} = E_{electrostatic} + E_{vander\ Waals} \quad (2.29)$$

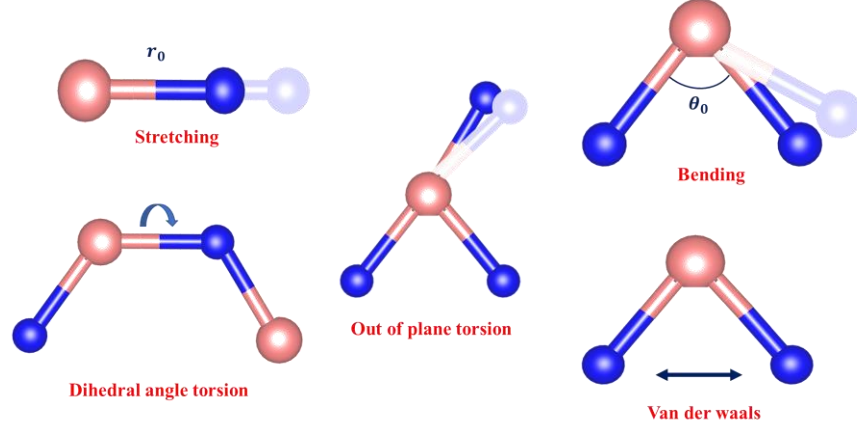


Fig. 2.4 Interatomic relative motions in molecular mechanics.

The Lennard Jones interactions (Rahman, 1994) or van der Waal's interactions are given by,

$$E_{ij} = 4\varepsilon_{ij} \left[\left(\frac{\sigma_{ij}}{r_{ij}} \right)^{12} - \left(\frac{\sigma_{ij}}{r_{ij}} \right)^6 \right] \quad (2.30)$$

where the equilibrium spacing parameter σ of the Lennard-Jones potential was considered to be the arithmetic mean of the individual parameters of the respective atom types and depth parameter ε was taken to be the geometric mean of the values of the respective atom types. The r is the distance between the two nonbonding atoms i and j . The exact functional form of a potential field depends on the type and condition of the simulation. The all-atom potential fields provide the parameters for each and every type of atom in a system, while the united-atom potential fields stipulate parameters only for specific types of atoms (Sun, 1998).

In the literature, Morse potential, reactive empirical bond order (REBO) potential, adaptive intermolecular reactive empirical bond order (AIREBO) potential fields are being used to simulate graphene and CNTs (Rao *et al.*, 1995; Sinnott *et al.*, 1999; Shen *et al.*, 2010). The REBO model is a function for calculating the potential energy of covalent bonds and interatomic force. Despite numerous successful applications of first generation REBO

potential function, its several drawbacks have been reported that are rectified in an extension of Brenner's potential was proposed by Stuart *et al.*, 2000. It is called the AIREBO potential force field.

2.2.8 AIREBO potential force field

The adaptive intermolecular reactive empirical bond order (AIREBO) potential was proposed by Stuart *et al.* in 2000. In AIREBO potential, both the repulsive and attractive pair interaction functions in REBO functions are modified to fit bond properties. The long-range atomic interactions and single bond torsional interactions are also included. AIREBO has been successfully applied to study the properties of graphene (Pregler *et al.*, 2007; NG *et al.*, 2012). In AIREBO potential, the potential energy (E) of an atomic configuration consists of three terms:

$$E = \frac{1}{2} \sum_i \sum_{j \neq i} \left[E_{ij}^{REBO} + E_{ij}^{LJ} + \sum_{k \neq i,j} \sum_{l \neq i,j,k} E_{ijkl}^{TORSION} \right] \quad (2.31)$$

where E^{REBO} is REBO energy; this term in AIREBO potential gives the model its reactive capabilities which only describes the short-ranged C-C, C-H, and H-H interactions ($r < 2 \text{ \AA}$). Further, E^{LJ} is Lenard-Jones energy; this term adds non-bonded interactions,

$$E_{ij}^{LJ} = 4\epsilon_{ij} \left[\left(\frac{\sigma_{ij}}{r} \right)^{12} - \left(\frac{\sigma_{ij}}{r} \right)^6 \right] \quad (2.32)$$

where the ij indices indicate the chemical species (C or H) of two interacting atoms; ϵ_{ij} and σ_{ij} are the well-depth energy and the distance at which pair interaction energy goes zero, respectively; and $E^{TORSION}$ is Torsion energy which describes the dihedral angle preference in hydrocarbon configurations.

2.2.9 Molecular dynamics parameters

Timestep: The length of time between two consecutive iterations in a MD simulation is called the time step. A time step should be less than 10% of the vibration period of an atom, and timestep of 0.5 fs to 0.8 fs provides excellent results for a carbon-based structure (Arachchige, 2012; Kundalwal and Choyal, 2018). However, researchers used a time step of 1 fs to perform MD simulation for graphene (Simons *et al.*, 2010; Borodin *et al.*, 2011). The selection of timestep depends on the computational efficiency and required accuracy of the simulations. The larger value of time steps increases the computational efficiency, while it reduces the accuracy of the simulations.

The smaller time steps may improve the accuracy of the simulations. Therefore, the time step controls the trade-off between computational efficiency and accuracy in the MD simulations. If the value of timestep is too large, then the system might become unstable. First, we check the equilibration of our system with a timestep of 0.001 ps (1 fs) for the simulation time of 1 ns. After running the simulation up to 1 ns and 2 ns, we found that the system is very well equilibrating when simulating for 1 ns with a timestep of 0.001 ps. So, after that, we run our all-MD simulations with a timestep of 1 fs and running up to 1 ns to get reliable results.

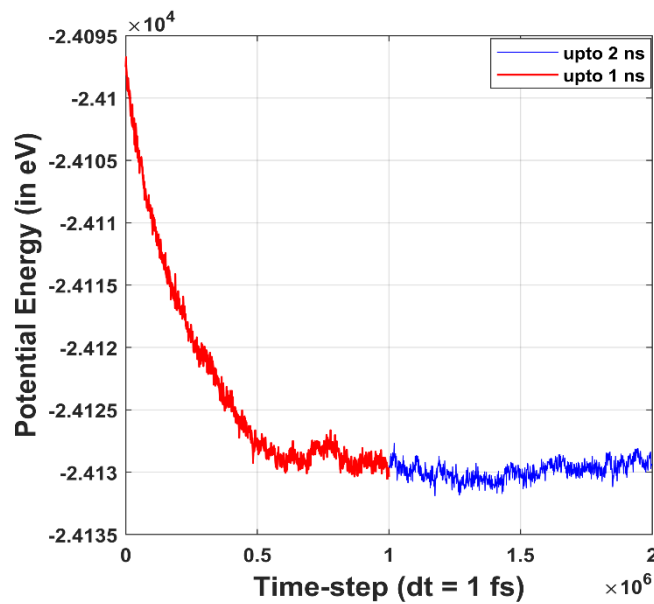


Fig. 2.5 Equilibration of PE vs no. of timestep (1 fs).

Periodic boundary conditions:

The term periodic boundary condition (PBC) (Allen, 2004) refers to the simulation of structures consisting of a periodic lattice of identical subunits. The effects of edges in the systems such as graphene layer should be eliminated in MD simulations to visualize the effect of strain and concentration of defects at the center of the graphene layer. Therefore, an extremely large system of graphene sheets can be simulated via MD simulations by ensuring that the edges and surfaces have a negligible effect, but this approach is computationally expensive. To reduce the computational efforts, PBCs in the MD simulations are the most efficient

method to simulate an infinitely large system. In PBCs, the cubical simulation box was replicate throughout space to form an infinite lattice as shown for a 2D case in Fig. 2.6. During the MD simulations, when an atom moves in the central box, then its periodic images in every other box also move exactly in the same way. Thus, when an atom leaves the box during the simulation, then it is replaced by an identical particle that enters from the opposite side, so the number of particles/atoms in the central box remains the same, and the system under consideration does not possess any edges.

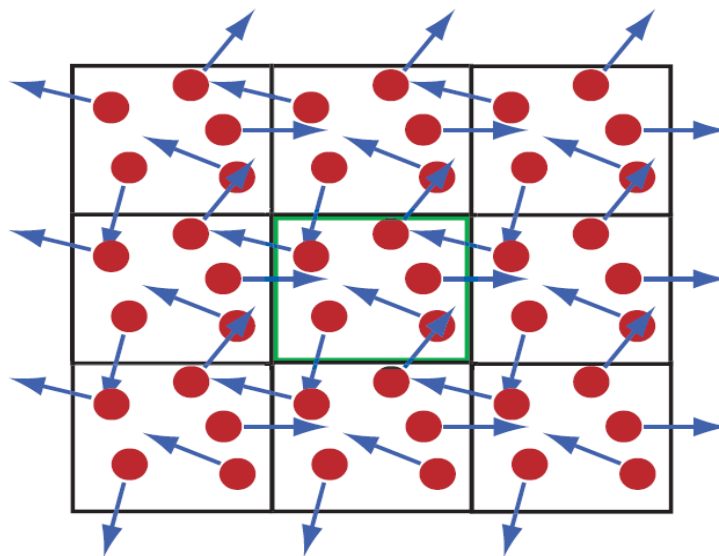


Fig. 2.6 Graphical representation of the PBCs of the middlebox. The arrows indicate the directions of the velocities of atoms. The atoms in the middlebox can interact with atoms in the neighboring boxes without having any boundary effects.

2.2.10 MD simulator

All the MD simulations were performed in LAMMPS. The Large-scale Atomic/Molecular Massively Parallel Simulator (LAMMPS) is a classical MD simulation software widely used in various applications at the atomistic level (Plimpton, 1995). It allows parallel particle simulations at the atomic, meso, and continuum scales. It allows to simulate atomic, chemical, or biological models at a microscopic scale. LAMMPS was developed at the Sandia National Laboratories and is written in C++. It is free and open-source software that continues to be updated by Sandia National Laboratories (Plimpton, 1995) and other researchers worldwide.

The MD simulator LAMMPS requires multiple script to perform the MD simulations, such as input script, coordinates of the atom in the system, and potential field. The formulation of the LAMMPS input script is shown in Fig. 2.7, and this script

can be divided into four sections: initiation, atom definition, setting, and running. The boundary conditions and units of the MD simulation are set in the initialization part of the input script. Different units and boundary conditions are available in the LAMMPS package. The use of metal units is mandatory for the AIREBO potential field for the MD simulations. In the metal units, the units of time, distance, and energy are picoseconds (ps), Angstroms (Å), and electron-volts (eV), respectively. The choice of boundary condition depends on the type of simulation and can be chosen as periodic and non-periodic.

The atom coordinates (x , y , and z) and types are defined under the atom definition section. In all MD simulations, the atom coordinates are given in a different file. The input script calls for this file during its execution.

The simulation parameters, potential field coefficients, and output options are given in the third section of the input script. The basic simulation parameters, such as temperature, pressure, time, etc., are defined here. The temperature and pressure controlling methods are implemented in LAMMPS, such as Berendsen and Nose-Hoover methods. The thermodynamics ensemble is also implemented in the third section of the LAMMPS, such as NVE, NVT, and NPT ensembles. During simulation, LAMMPS allows to compute time and spatial averages of physical quantities, such as pressure, temperature, energies, stresses, etc., and separated text files can be obtained at specified time intervals.

The final section is the running of the simulations. During the simulation, LAMMPS allows to deform the simulation box. During the simulation, the nanostructure is also deformed along with the simulation box. The output of the MD simulation from the LAMMPS can be obtained as a “*log.lammps*” and “*dump.file*” files after the pre-specified number of time steps or a completion of run time.

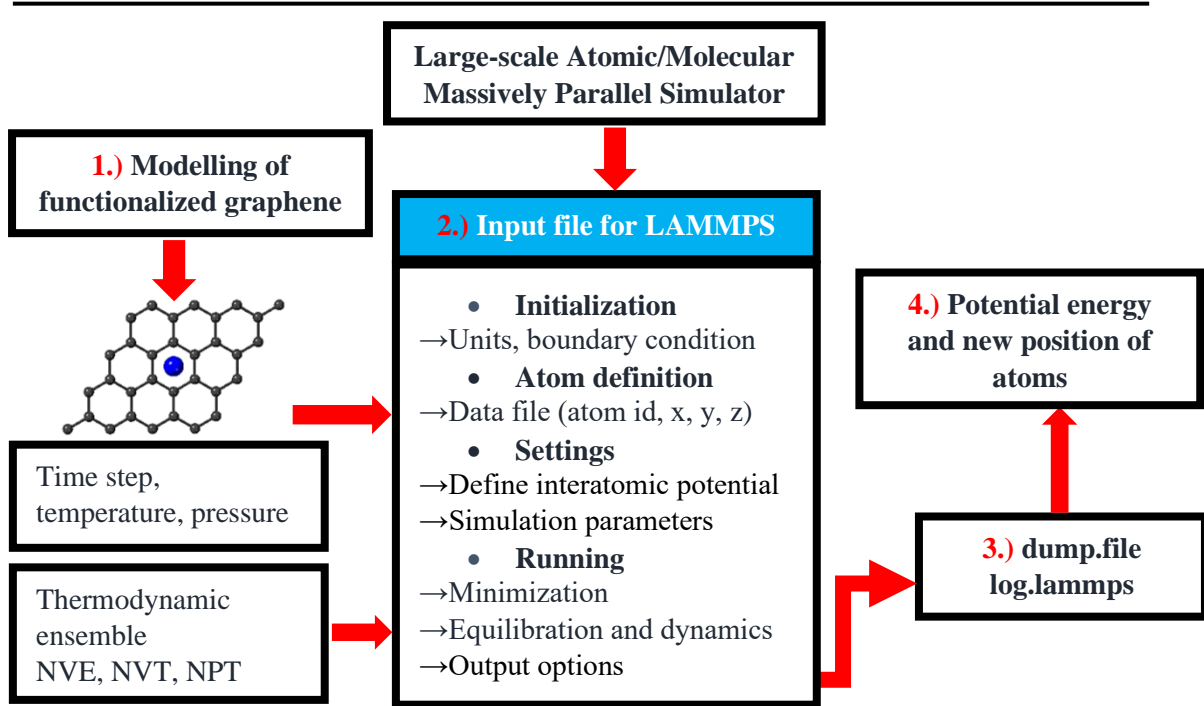


Fig. 2.7 The overview of LAMMPS

The output of LAMMPS contains all the position information pertaining to atoms at every timestep. However, LAMMPS does not have the functional visualization capability to display the various trajectories directly. Therefore, additional visualization software is required for analyzing the results obtained more easily. In this regard, the VMD (Dalke *et al.*, 1996) and OVITO (Stukowski *et al.*, 2020) software can be used to read the LAMMPS output data and render informative figures.

The theory behind this chapter will be used to give the overview of MD simulations and define the potential of graphene subjected to strain, and different vacancy defects on the storage of hydrogen in subsequent chapters. The next chapter discusses the effect of strain on the hydrogen adsorption capacity of the graphene sheets. How strains are provided to the sheet and the method of potential energy distribution to calculate the wt.% are also discussed in the next chapter.

Chapter 3

Effect of strain on wt.% of hydrogen stored on graphene

In this chapter, the hydrogen adsorption capacity of the graphene layer subjected to uniaxial strain is investigated using the MD simulations. The effect of strain on the storage of hydrogen at specified temperatures and pressure is studied. This chapter represents the methodology used to calculate the wt.% of hydrogen and how the sheet is subjected to strain. Also, the equilibration of the system is discussed.

3.1 Introduction

Graphene has captured massive response from researchers around the globe due to its exceptional mechanical, electrical, and thermal properties. Physisorption is a surface phenomenon; if the surface area is large, the physical adsorption is more. Graphene has a high SSA which makes it a potential candidate for the storage of hydrogen via physisorption. Providing a strain up to 10% can lead to structural deformation and it can store more wt.% of hydrogen as compared to pristine (Xue and Xu, 2010). A monolayer of graphene becomes chemically active by introducing the strain up to 10% (Surya *et al.*, 2012). Providing a strain to the graphene sheet, the system's d-level configuration changes, which changes the binding energy of the adsorbing elements and increases the hydrogen adsorption capability (Liao *et al.*, 2015). In general, strain modifies the atomic structural, mechanical, and chemical activity of 2D materials (Deng *et al.*, 2018).

From the literature, it can be concluded that graphene subjected to strain up to 10% can change its chemical activity and atomic structure, leading to increment in wt.% of hydrogen compared to pristine, and the elastic response is highly nonlinear for strain above 10% (Lee *et al.* 2008). Above all, studies were performed using the first principle calculations. In this chapter, MD simulations were performed to determine the effect of strain on the wt.% of hydrogen. The calculation of wt.% was performed with the help of the potential energy distribution.

3.2 MD modelling of graphene

MD simulations were performed in the current study using LAMMPS (Plimpton, 1995). The interaction energy of each atom was calculated using the AIREBO potential force field (Stuart *et al.*, 2000).

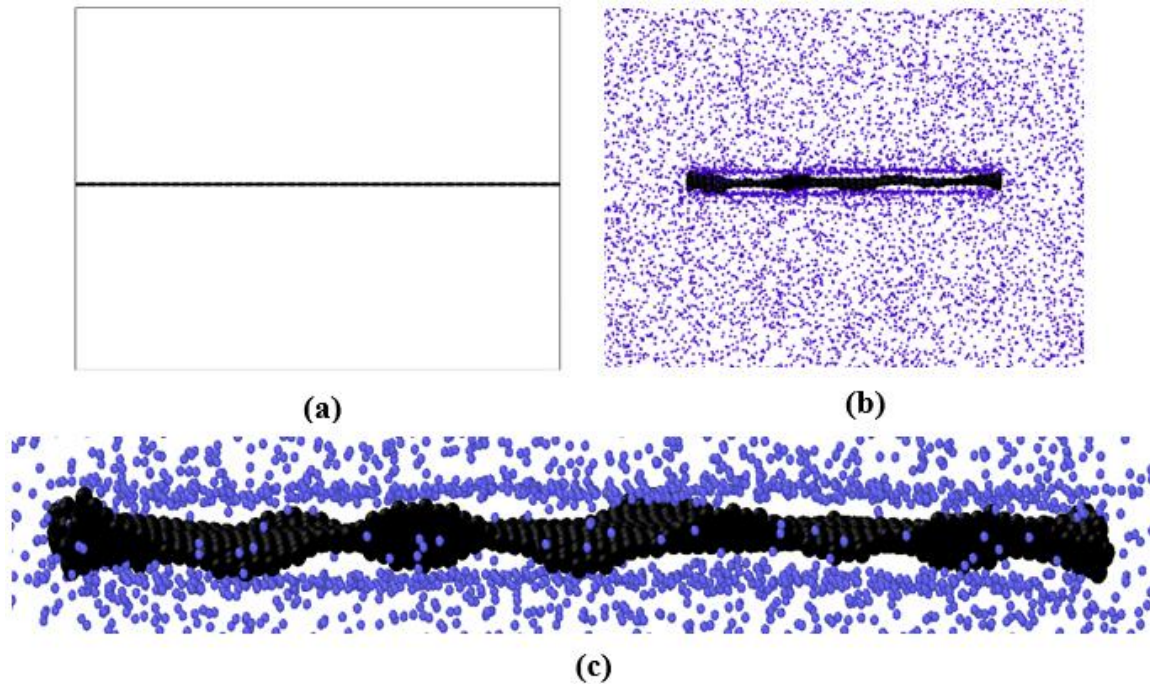


Fig. 3.1 Modelled graphene layer (black dots ●) and H₂ molecule (blue dots ●): (a) Initial system configuration with relaxed graphene, (b) after simulation time of 1 ns, and (c) adsorbed H₂ molecules around graphene layer.

Initially, a graphene layer of size 100 Å x 100 Å was modelled using the modelling software (VMD, Vesta). However, the modelled structure is not in its minimum energy configuration. Firstly, minimization and equilibration of the graphene layer were performed to obtain a relaxed graphene structure with minimum energy, as shown in Fig. 3.1(a). Further, Fig. 3.1(b) illustrates the graphene layer and hydrogen molecules after 1 ns, and Fig. 3.1(c) shows the adsorbed hydrogen molecules around the graphene layer. All simulations are performed with a time step size of 0.001 ps, with a simulation box size of 150 Å x 150 Å x 100 Å to encapsulate the accurate hydrogen adsorption dynamics. The optimized graphene structure was obtained by minimizing the system's energy using the conjugate gradient method. Initially, the modelled structure has some pre-stored stress, so a relaxation at low temperature (77 K) for 250 ps using the NVT and NPT ensembles was

carried out to obtain a stress-free graphene layer. After that, H₂ molecules were added randomly to the simulation box and further using the NPT ensemble we achieved the desired pressure and temperature. Then, an equilibration run of 1 ns under the isothermal and isobaric conditions was carried out to equilibrate the system. The above simulation steps were performed multiple times at each pressure and temperature to obtain results.

3.2.1 Strain engineering

After obtaining a stress-free/relaxed graphene layer, the armchair direction of the graphene was stretched. One end of the sheet (left side) was fixed, and the other end (right side) was free, as shown in Fig. 3.2. Then, the free edge of the graphene layer was displaced along the direction perpendicular to the edge. Initially, the C-C bond length was 1.42 Å, and the maximum elongation of the C-C bond in this study was set to the bond length of 1.562 Å; thus, a strain of 10% strain was provided. For providing a strain to the sheet, we used the fix move command to get desired strain. We started from the zero strain to take it up to a maximum of 0.1 in 10 steps. After each step, we equilibrated the system and calculated the wt.% of hydrogen. The method is described in the next section 3.2.2. In the subsequent steps, we increased the strain by 0.01 to achieve the maximum possible strain by maintaining the structural integrity of graphene. The strain (e) can be calculated as,

$$e = \frac{\text{Change in length}}{\text{Initial length}} = \frac{l-l_0}{l_0} \quad (3.1)$$

where, l = final C-C bond length in a graphene layer

l_0 = initial C-C bond length

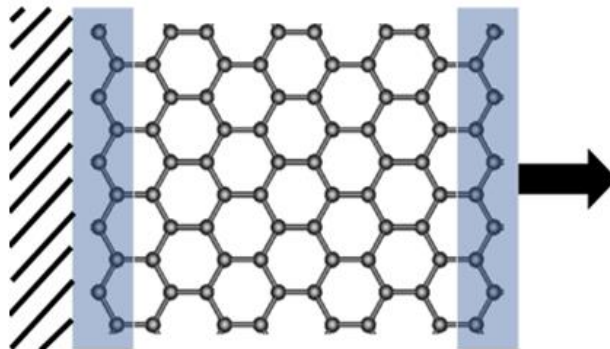


Fig. 3.2 Graphene layer under tension.

3.2.2 Gravimetric density (wt.%) calculations

The amount of H₂ molecules adsorbed was calculated by observing the hydrogen molecules' potential energy distribution. While running the simulations, H₂ molecules are physically adsorbed around the graphene layer, as illustrated in Figs. 3.1 (b) and (c). The potential energy of each of the hydrogen molecules was obtained in a separate data file from the output of LAMMPS. It was observed that the distribution of potential energy with the number of hydrogen molecules follows a pattern that the particle near the sheet had lower potential energy, indicating the hydrogen molecule is in a stable position. Therefore, it was considered that the H₂ molecules having potential energy lower than -0.012 eV are adsorbed on the sheet (Luhadiya *et al.*, 2020). Figure 3.3 shows the potential energy distribution of each H₂ molecule around the graphene layer at 77 K and 10 bar with a probabilistic curve fitting. It was revealed that a local minima point exist in the energy distribution; below this minimum point, adsorbed H₂ molecules lie, as shown in Fig. 3.3 (a). For the validation of such adopted method, the H₂ molecules belonging to the adsorbed potential energy were segregated and it can be observed from Fig. 3.3 (b) that they surround the sheet as visualized (side view). Carbon atoms of graphene were kept hidden for clarity. Then, the numbers of adsorbed hydrogen molecules were counted.

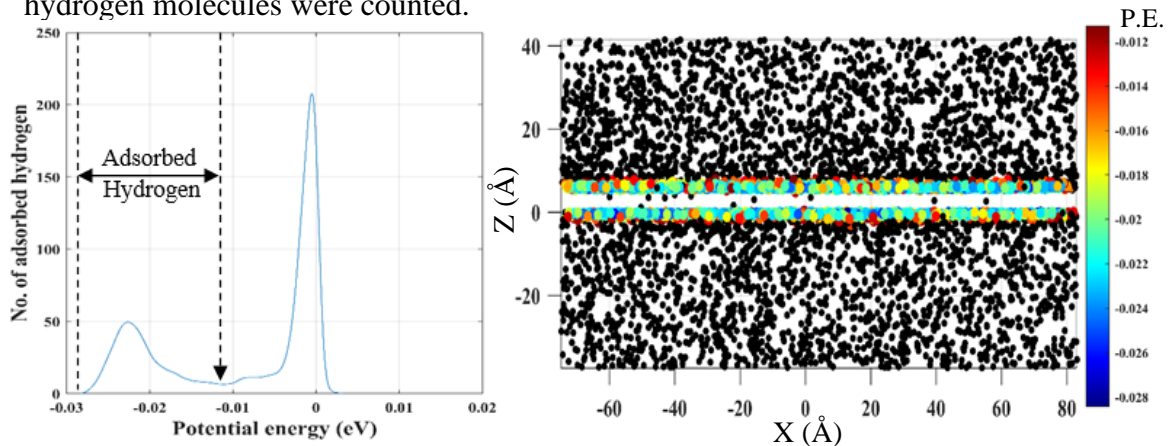


Fig. 3.3 (a) Potential energy distribution of hydrogen molecules, and (b) spatial distribution of potential energy of H₂ molecule at 77 K and 10 bar.

The gravimetric density (wt.%) of the storage system was calculated using Eq. (3.2). Then, an average of wt.% of the equilibrated system's last 50 -100 timesteps was used to obtain an accurate gravimetric density. To the best of our knowledge, no other study has used this method to observe the adsorption phenomenon using the MD simulations.

$$wt. \% = \frac{m_h n}{m_h n + m_c N} \times 100 \quad (3.2)$$

where m_h is mass of hydrogen molecule, m_c is mass of carbon atom, n is total number of adsorbed hydrogen molecules, and N is total number of carbon atoms in a graphene layer.

Adsorption energy can be calculated by,

$$E_{adsorption} = E_{Graphene+H_2} - (E_{Graphene} + E_{H_2}) \quad (3.3)$$

where $E_{Graphene}$ is the potential energy of graphene layer, E_{H_2} is the potential energy of hydrogen molecule, and $E_{Graphene+H_2}$ is the potential energy of the graphene layer with adsorbed hydrogen molecules. It should be noted that the adsorption energies calculated are negative values which signifies the strength of the attraction between the graphene layer and hydrogen molecules. A higher value indicates a stronger attraction among the adsorbate and adsorbent.

3.3 Effect of strain

The effect of strain on hydrogen storage capacity of graphene layer was studied using MD simulations. The strain was provided in the armchair direction of graphene. Figure 3.4 represents the variation of wt.% of hydrogen adsorption of graphene layer with strain. To calculate the strain, we used Eq. (3.1). Once the required strain was provided, the system was equilibrated at the desired temperature and pressure. Then, the wt.% was calculated using the method provided in section 3.2.2 at 77 K temperature and 10 bar pressure. Figure 3.4 depicts an increase in the wt.% of hydrogen adsorption of the strained pristine graphene from 5.42 to 6.28 with an increasing strain. The strain provided to graphene increases the chemical activity and makes it more chemically active for hydrogen adsorption, change in the bandgap levels, catalytic properties, and stretching of the graphene significantly influence the interaction between the adsorbents (Surya *et al.* 2012, Zhou *et al.* 2010, Katin *et al.* 2017). Simultaneously, the C-C bond length also increases, due to which the total surface area increases as physisorption is a surface phenomenon, the wt.% increases with the strain increment. We have also performed the tensile testing of pristine; we found that the pristine sheets can bear strain up to 20% without failure, but with defects, the tensile strength decreases, and we can conclude from figure 4.9 that the failure point is at 0.2 strain, but in case of defected graphene multiple failure points are observed, which restricts us to provide a strain of

more than 10%, for a safe design and to avoid the mechanical failure during adsorption. The fracture of the graphene sheet (**Fig. A1-A6**) is explained in detail in the appendix section of the thesis. Table 3.1 contains the some of the results from the literature on hydrogen storage when decorated graphene subjected to strain and sheet with biaxial strain. Note that the system equilibration is very important for an accurate simulation as the effect of pressure and temperature on wt.% was significant. Figure 3.5 represents the evolution of the gravimetric density and pressure with no. of timesteps. It can be seen from Fig. 3.5 that wt.% and pressure both are equilibrating very well with a mean value of 5.5 and 10 bar, respectively, with a time step size of 0.001 ps and a total simulation run time of 1 ns.

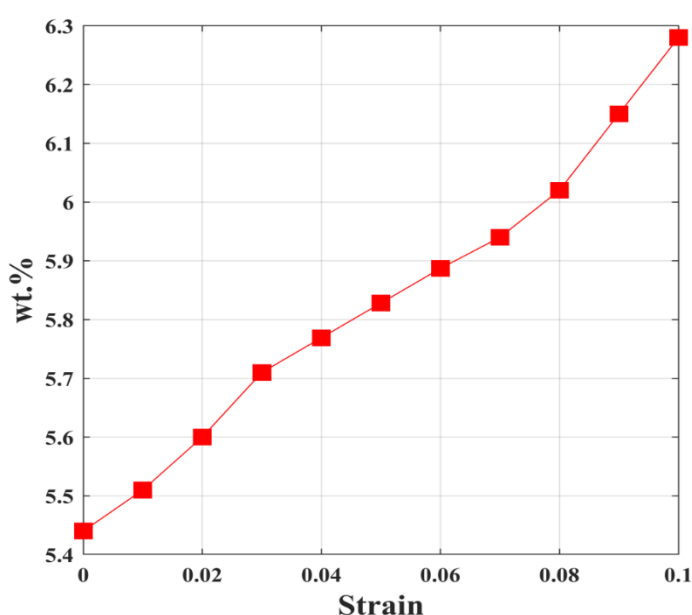


Fig. 3.4 Variation of wt.% of hydrogen adsorption on graphene with strain at 77 K and 10 bar.

Table 3.1 Data related to studies performed on the strained graphene for hydrogen storage

Methodology	Results	Reference
Asymmetric strain ($x = 7.5\%$, $y = 10\%$) with Lithium dopant	12.12 wt.% of hydrogen	Hussain <i>et al.</i> (2012)
A tensile strain of 10% with Li (Ti) as a dopant	15.4 (9.5) wt.% of hydrogen	Zhou <i>et al.</i> (2010)
A biaxial strain of 10%	The binding energy of hydrogen on graphene was improved	Xue and Xu (2010)

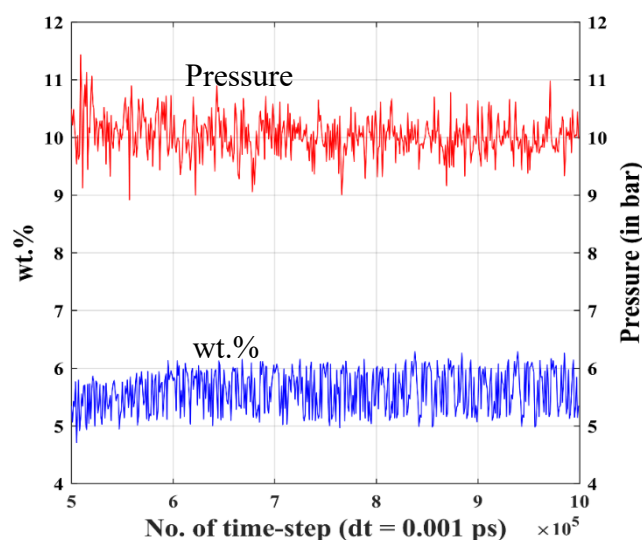


Fig 3.5 Variation of wt.% of hydrogen adsorption on graphene and pressure with no. of time steps

3.4 Conclusions

In this chapter, we have studied the effect of strain applied along the armchair direction of graphene on wt.% of hydrogen storage using the MD simulations. We have found that the wt.% of hydrogen storage increases with the increment in strain up to 10%, and maximum of 6.28 wt.% is achieved at 0.1 strain, 10 bar and 77 K.

- Development of potential energy method first time in literature. It is found to be a novel method used for the calculation of gravimetric density of hydrogen.
- Plotted the potential energy distribution of hydrogen molecules and obtained a point of local minima at -0.012eV of potential energy.
- Providing a strain to the sheet up to 10%, gravimetric density increases which further can be increased up to 16% as compared to pristine sheet at same temperature and pressure conditions.
- Graphene under strain modifies its bond lengths due to which its chemical activity improves, and we obtain a higher wt.% of hydrogen.
- Pressure and wt.% of hydrogen with respect to number of timesteps are equilibrating very well for longer duration on the order of ns.

Chapter 4

Effect of defects on wt.% of hydrogen stored on graphene

This chapter investigates the effect of different types of defects in the graphene sheet on the storage of hydrogen via MD simulations. Different types of vacancy defects in the graphene sheet were modeled and a defect type was identified which showed a greater wt.% of hydrogen storage. We also investigated the effect of defects on the strength of graphene.

4.1 Introduction

Graphene is a 2D material with a considerable potential to be used for the storage of energy due to its unique properties, as discussed in the previous chapters. The graphene can be synthesized by various techniques, and during its synthesis, produced graphene usually consist of different types of inherent defects. The possible point vacancy defects are monovacancy (MV), Stone Wales (SW) defects, and double vacancy (DV) defects. These defects have a more significant impact on the storage of hydrogen as well as on the strength of the graphene. The review of the literature in chapter 1 reveals that the defective sheet can have more active sites for the storage of hydrogen and can hold more hydrogen as compared to the pristine sheet.

From the literature survey, we have found that the investigation on defected sheet is majorly done with the help of first principle methods and some of the experimental studies also exist. To the best of our knowledge, there is a no single MD study on the large-scale defected graphene for hydrogen storage; moreover, the effect of defects on the critical stress and strain of graphene is not yet studied. In this chapter, we discuss the influence of different types of defects on the gravimetric density, calculation of the average adsorption energy, and the strength of graphene containing the different types of defects.

4.2 MD modelling of defected graphene

MD simulations were performed to determine the wt.% of hydrogen storage on the graphene containing different types of defects. In general, five types of defects have

been found in the graphene after the synthesis. The defects can be characterized in two ways: the absence of atoms and geometrical structure of defects.

Types of defects based on absence of atoms:

- MV defect – absence of one atom
- SW defect – no removal or addition of atom; rotation of C-C bond by 90^0
- DV defect – absence of two adjacent atoms

Based on geometrical structure of defect:

- SW defect – 55-77 defect
- DV defect – 5-8-5, 555-777, and 5555-6-7777 DV defect

The particle irradiation process of solid nanostructures with energetic particles such as electrons or ions is a well-known technique for creating atomic defects in the material intentionally and altering their properties (Banhart *et al.*, 2011; Deretzis *et al.*, 2012). However, the defects also often occur randomly during the synthesis of graphene. We intend to study how different types of defects and their concentration influence the hydrogen adsorption capability of graphene. The vacancy concentration (ρ) is calculated using the following relation (Kundalwal *et al.*, 2018; Kothari *et al.*, 2018):

$$\rho = \frac{N_r}{N} \times 100 \quad (4.1)$$

where N_r is the number of removed C atoms and N is the total number of atoms in the pristine graphene. While creating a defect, unless otherwise mentioned, the carbon atoms were removed from the central region of graphene layer, as shown in Fig. 4.1. This figure shows the pristine and different defected graphene sheets containing MV or SW or DV defects. The MV defect is created when one C atom is moved from its lattice position. In SW defect, any C-C bond is rotated by 90^0 , creating heptagon and pentagon rings. When two adjacent MV combine or two adjacent C atoms are removed simultaneously, a 5-8-5 DV defected graphene is obtained. Further, when the one side of the octagon formed in 5-8-5 is rotated by 90^0 , then 555-777 DV defect is created, and finally, when the other side of the octagon is also turned by 90^0 , then 5555-6-7777 DV defect is created.

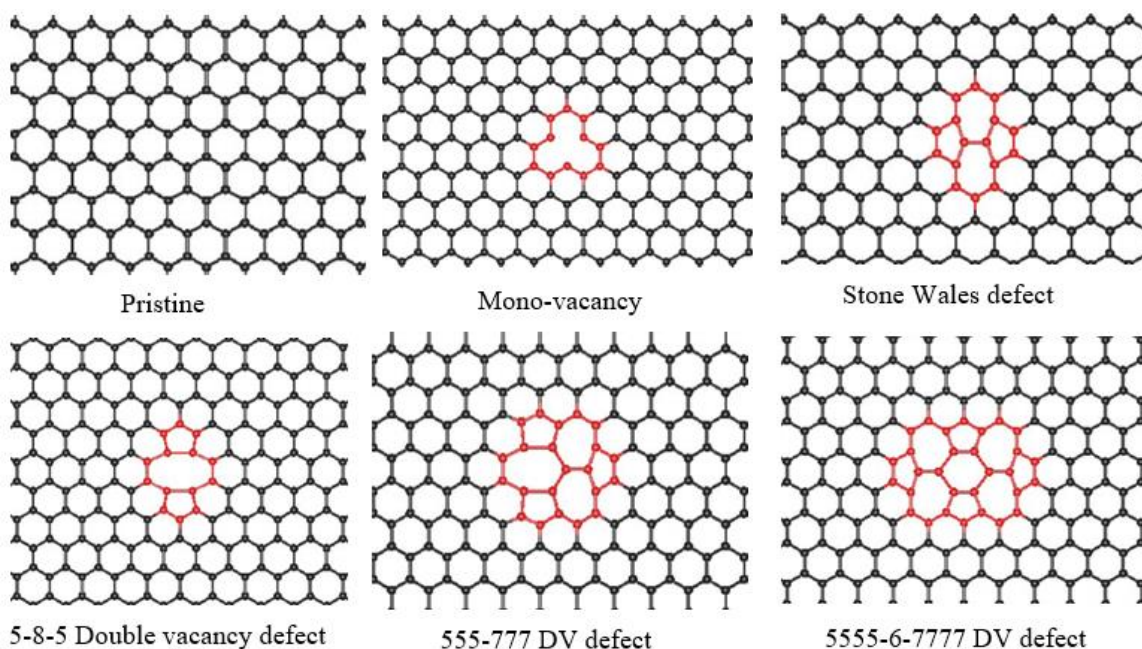


Fig. 4.1 Pristine and defected graphene sheets.

Table 4.1: The bond lengths of pristine and defected sheets

S. No.	Sheet	Average bond length (in Å)
1	Pristine	Initially - 1.42 After 10% strain – 1.514
2	MV defected	Initially - 1.4668
3	SW (55-77) defected	Pentagon – 1.432 Heptagon – 1.399
4	5-8-5 DV defected	Pentagon – 1.599 Octagon – 1.704
5	555-777 DV defected	Pentagon – 1.57 Heptagon – 1.559
6	5555-6-7777 DV defected	Pentagon – 1.449 Hexagon – 1.411 Heptagon – 1.43

Table 4.1 contains the data of average bond lengths of the pristine and defected graphene sheets. The average bond lengths were calculated after the energy minimization of the graphene or a structure with minimum energy.

4.3 Effect of defects

As mentioned earlier in section 4.2, the presence of vacancies causes stress concentration in the vicinity of defect region in the system and alters its chemical reactivity (Denis *et al.*, 2013). Figure 4.2 (a) represents the variation of gravimetric density with pressure for pristine graphene at a constant temperature. The wt.% increases with an increase in pressure at a 77 K temperature, and at higher pressures (above 50 bar), the wt.% becomes invariable with the rise in pressure. So, it can be concluded that the saturation state was achieved at the given temperature. Figure 4.2 (b) represents the variation of average adsorption energy with pressure at a constant temperature. From the respective figure, we can conclude that at a lower temperature, the magnitude of average adsorption energy is more as compared to that at a higher temperature. If the magnitude of average adsorption energy is more, the stronger is the interaction between the interacting elements, and hence the wt.% is more at a lower temperature. As the magnitude of average adsorption energy increases with an increase in pressure, it can hold more H₂ molecules. With the pristine sheet, a maximum value of 6.55 wt.% of H₂ at 77 K temperature and 1.17 wt.% of H₂ at 300 K are achieved. The average adsorption energy calculation of hydrogen molecules on the graphene layer was found to be -0.0402 eV at a temperature of 77 K (Yadav *et al.*, 2014; Costanzo *et al.*, 2012). Also, 0.6 wt.% of H₂ at 77 K and 1 bar pressure, and 0.083 wt.% of H₂ at 300 K and 1 bar pressure (Ma *et al.*, 2009) were achieved. At higher temperatures, the kinetic energy of molecules increases, leading to the desorption of H₂ molecules; hence, at 300 K, a lower wt.% is obtained.

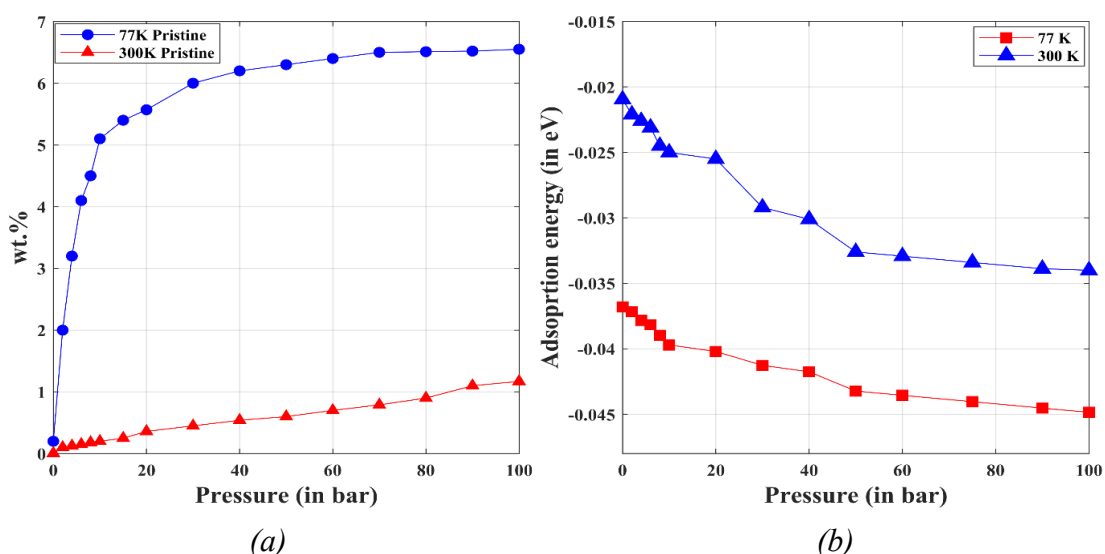


Fig. 4.2 (a) Adsorption isotherm and (b) average adsorption energy vs pressure for pristine graphene.

We have discussed different types of defects in graphene that can occur during synthesis earlier. Figure 4.3 demonstrate the effect of defects on the hydrogen adsorption capacity of the defected graphene layer. This figure also represents the comparison of gravimetric density of graphene containing 1% of MV concentration with the pristine graphene at various pressures and temperatures. It is observed that the wt.% of H₂ over the graphene containing the MV is more than pristine, and with increment in pressure, the wt.% of H₂ increases. The graphene containing MV defects achieve a maximum value of 9.3 wt.% of H₂ at 77 K temperature, and 2.208 wt.% of H₂ at 300 K, at a constant pressure of 100 bar. In comparison, graphene containing MV defects achieves a minimum value of 0.25 wt.% of H₂ at 77 K and 0.00625 wt.% of H₂ at 300 K, at a constant pressure of 0 bar. The average adsorption energy of the H₂ molecule adsorbed on graphene was found to be -0.3282 eV at a temperature of 77 K (Yadav *et al.*, 2014). With 1% of MV concentration defect, the percentage rise in wt.% is around 42% compared to the pristine graphene at 77 K and 100 bar.

Figure 4.4 compares the gravimetric density of H₂ of graphene layer containing 1% of SW concentration with the pristine graphene at different pressures and constant temperature. This figure depicts that the H₂ adsorption wt.% of the graphene with SW defect is more than the pristine graphene. In case of graphene containing the SW defects at a pressure of 100 bar, a maximum value of 7.23 wt.% of H₂ at 77 K and 2.1043 wt.% of H₂ at 300 K temperature is obtained, and a minimum value of 0.208 wt.% of H₂ at 77 K and 0.00561 wt.% of H₂ at 300 K at a pressure of 0 bar is obtained. The average adsorption energy of hydrogen molecule on graphene with SW defect was found to be -0.04409 eV at a temperature of 77 K (in literature, the value is -0.0610 eV; Yadav *et al.*, 2014; Costanzo *et al.*, 2012). With 1% of SW defect concentration, the percentage rise in wt.% of H₂ is around 10.4% compared to the pristine graphene at 77 K and 100 bar.

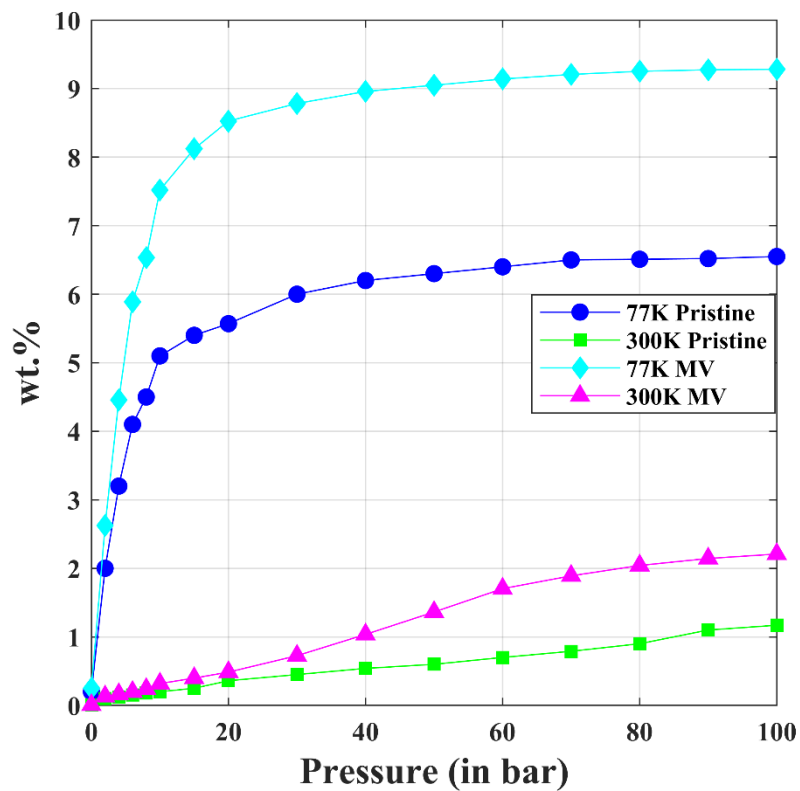


Fig. 4.3 Adsorption isotherm for MV

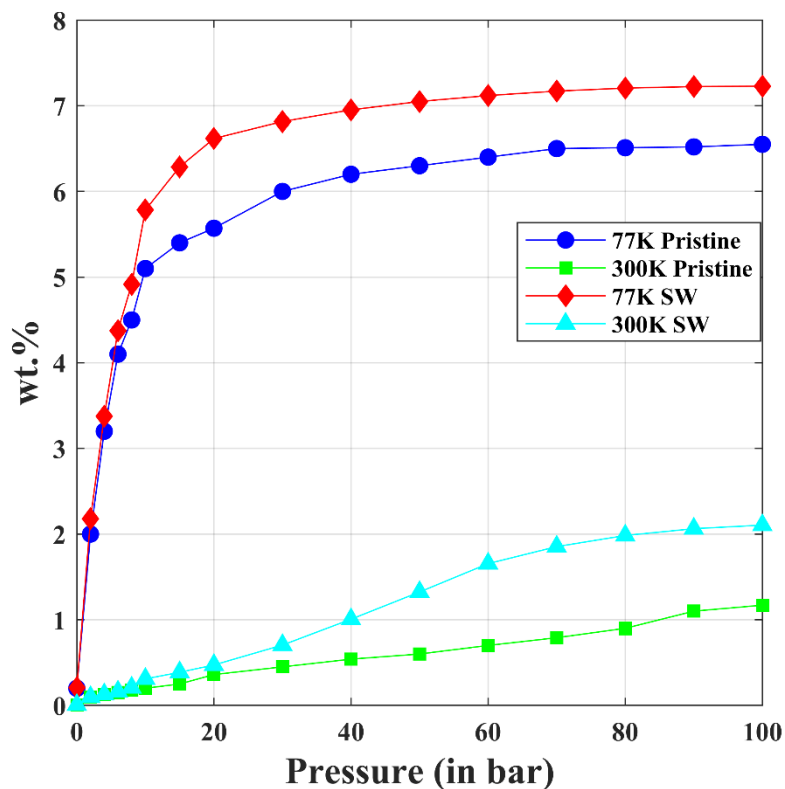


Fig. 4.4 Adsorption isotherm for SW

Figure 4.5 represents the comparison of the hydrogen gravimetric density of the graphene layer containing 1% concentration of 5-8-5 DV defect with the pristine graphene at different pressures and constant temperature. It is observed that the adsorption wt.% of H₂ molecules is more in 5-8-5 DV defect as compared to pristine case. Graphene layer containing the 5-8-5 DV defects can adsorb a maximum value of 8.763 wt.% of H₂ at 77 K and 2.3098 wt.% of H₂ at 300 K temperature, and the minimum value of 0.234 wt.% of H₂ at 77 K and 0.0085 wt.% of H₂ at 300 K, at a pressure of 0 bar. The average adsorption energy of the H₂ molecule for adsorption on 5-8-5 DV graphene is -0.0956 eV, which is higher in magnitude than the average adsorption energy for the pristine graphene. With 1% concentration of 5-8-5 DV defect, the percentage rise in wt.% of H₂ is around 34% compared to the pristine graphene at 77 K and 100 bar.

Figure 4.6 shows the comparison of gravimetric density of graphene layer containing 1% concentration of 555-777 DV defect with the pristine graphene at different pressures and constant temperature. This figure depicts that the wt.% of adsorbed H₂ molecules is higher for the defected graphene than pristine graphene. The graphene layer containing 555-777 DV defects adsorbs a maximum value of 8.17 wt.% of H₂ at 77 K and 3.006 wt.% of H₂ at 300 K temperature, and a minimum value of 0.21 wt.% of H₂ at 77 K and 0.00918 wt.% of H₂ at 300 K, at 0 bar pressure. The average adsorption energy calculation of adsorbed H₂ molecule on 555-777 DV graphene is -0.07929 eV at a higher adsorption temperature than pristine graphene. With 1% of 555-777 DV defect concentration, the percentage rise in wt.% is 25% compared to the pristine graphene at 77 K and 100 bar.

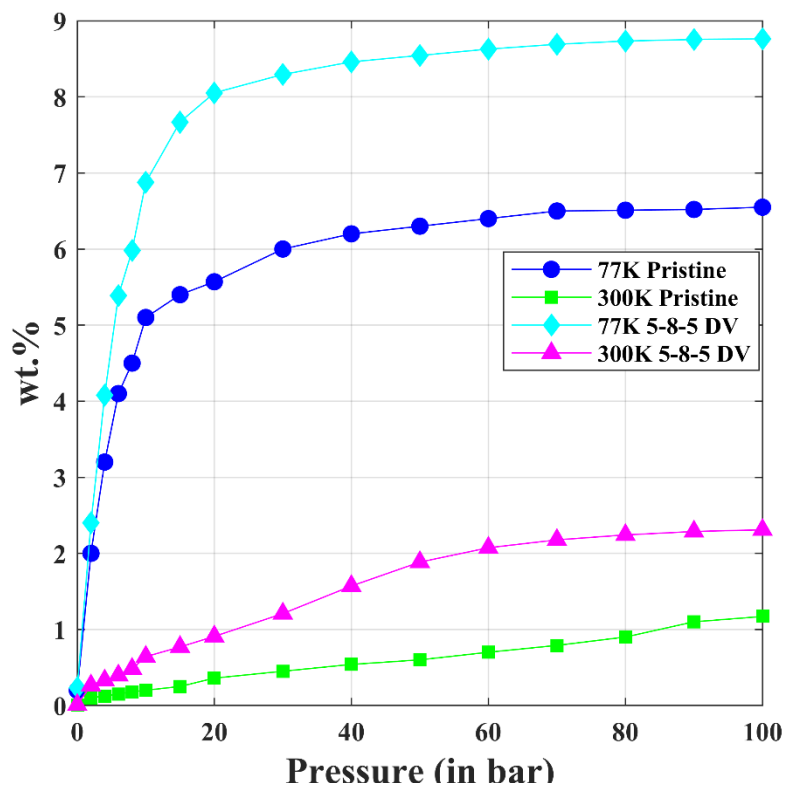


Fig. 4.5 Adsorption isotherm for 5-8-5 DV

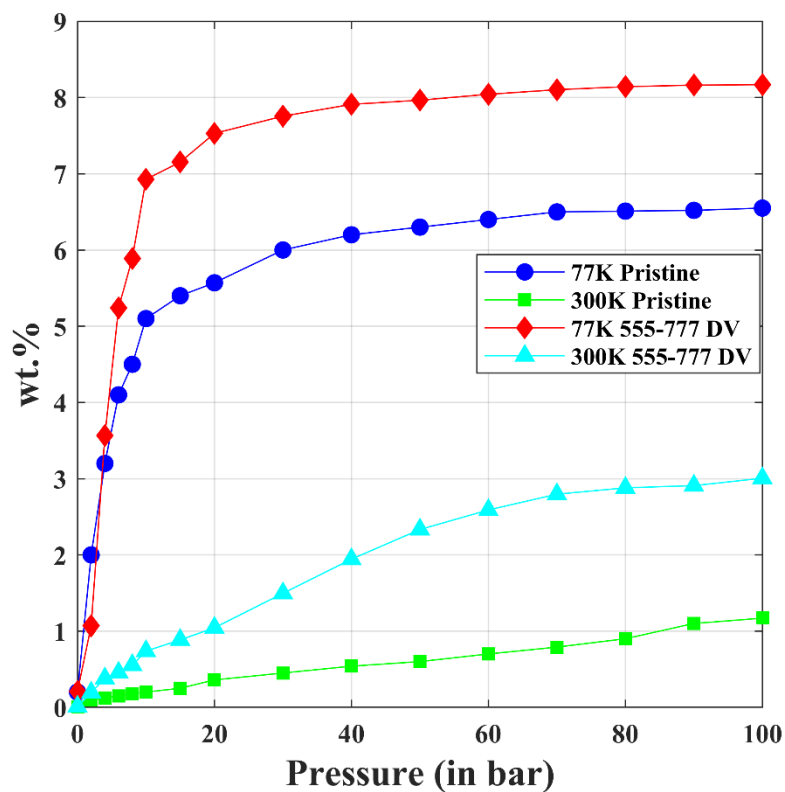


Fig. 4.6 Adsorption isotherm for 555-777 DV

Figure 4.7 represents the comparison of gravimetric density of graphene layer containing 1% concentration of 5555-6-7777 DV defect with the pristine graphene at different pressures and constant temperature. Graphene having the 5555-6-7777 DV defects at 100 bar pressure adsorbs a maximum value of 8.6205 wt.% of H₂ at 77 K and 3.096 wt.% of H₂ at 300 K temperature, and a minimum value of 0.218 wt.% of H₂ at 77 K and 0.00991 wt.% of H₂ at 300 K. The average adsorption energy of adsorbed hydrogen molecule on 5555-6-7777 DV graphene is -0.08403 eV, which is very much comparable to pristine graphene and a possible reason to adsorb more hydrogen at a temperature of 77 K. With 1% concentration of 5555-6-7777 DV defect, the percentage rise in wt.% is 31% compared to the pristine graphene at 77 K and 100 bar.

In the previous sets of results, we have compared the adsorption of hydrogen over defected graphene with pristine graphene. Here, we discuss the adsorption and desorption isotherm for defected graphene with pristine graphene. Figure 4.8 (a) represents the comparison of adsorption wt.% of H₂ on pristine graphene to the defected graphene at a temperature of 77 K. It can be concluded from Fig. 4.8 that the defective graphene adsorbs more hydrogen molecules compared to the pristine graphene. The MV defected graphene shows the maximum wt.% of H₂ compared to other defects. This is attributed to the MV's activity towards the adsorption of H₂ is more compared to different types of defects considered herein. Also, the average adsorption energy calculation suggests that the MV's had the highest magnitude of average adsorption energy compared to the other possible defects. Figure 4.8 (b) represents the isotherm at 300 K showing the comparison of gravimetric density of H₂ molecule on graphene with various defects to the pristine graphene. This figure depicts that the graphene with the MVs and SW defects has a greater desorption ability than other defects. A maximum value of 1.17 wt.%, 2.2083 wt.%, 2.1043 wt.%, 2.3098 wt.%, 3.006 wt.%, and 3.096 wt.% is achieved at a pressure of 100 bar for pristine, MV, SW, 5-8-5 DV, 555-777 DV, and 5555-6-7777 DV defected sheet, respectively.

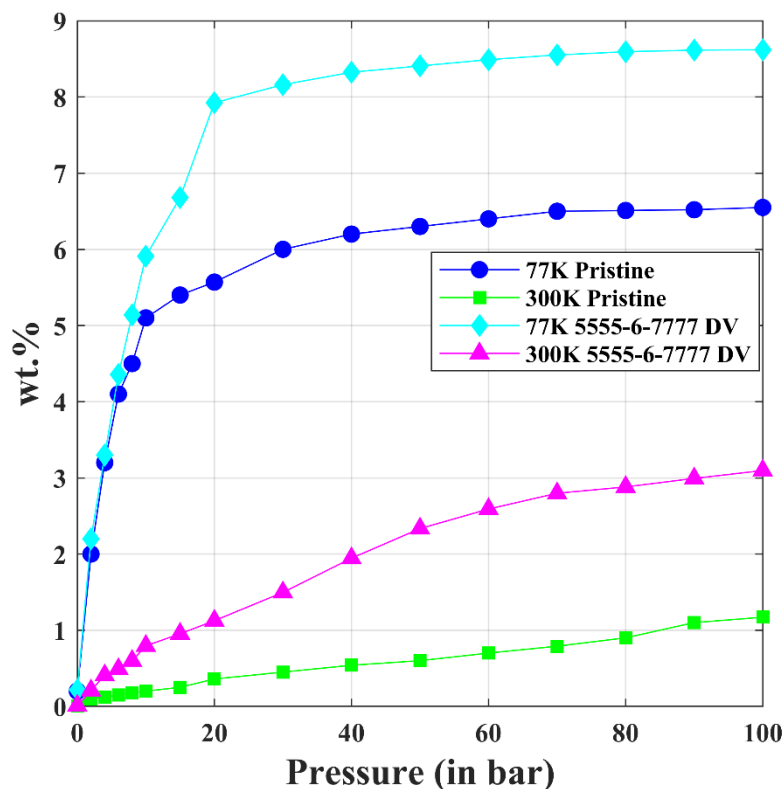


Fig. 4.7 5555-6-7777 DV defected sheet isotherm

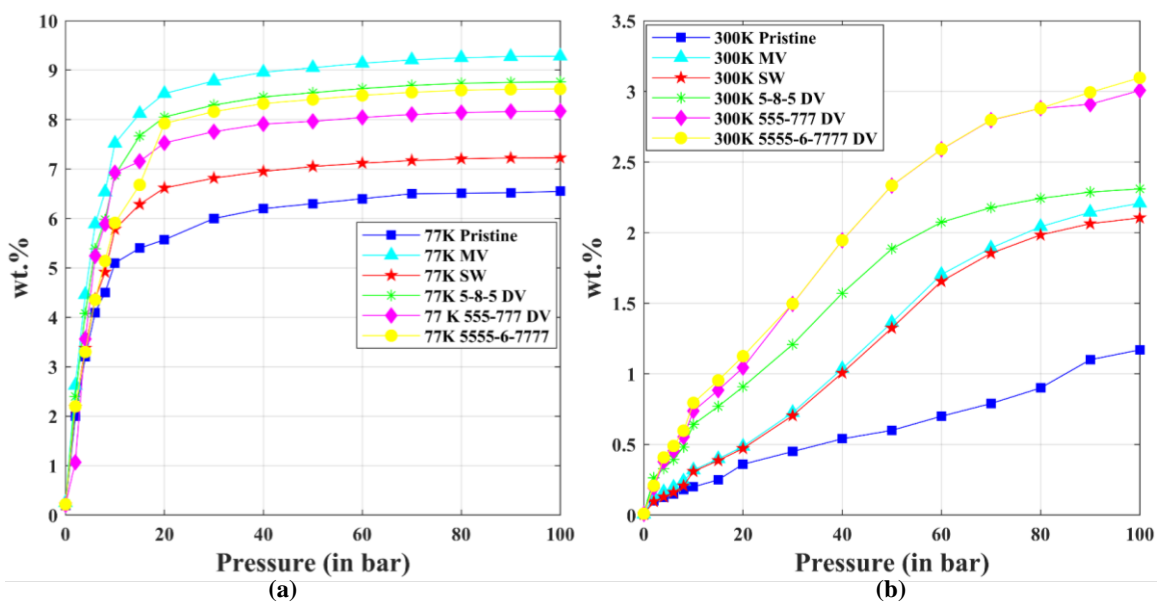


Fig. 4.8 Isotherm curves at (a) 77 K and (b) 300 K for graphene with different defects.

Further, it is essential to analyze the behavior of stress and strain of pristine and defected graphene. Figure 4.9 represents the variation of stresses induced in the graphene with 1% defect with strain. The critical stress and critical strain values were found to be 134.83 GPa and 0.2, respectively, for the pristine graphene, as shown in figure 4.9. Figure 4.8 (a) shows that the defective graphene has a higher ability to adsorb the H₂ molecules than pristine graphene, but the critical stress and strain values are reduced. The critical stress and strain values of defected graphene are reduced by 30% and 31%, respectively, for a 1% defect concentration. If the concentration of defects increases further, the maximum strength carrying ability of defected graphene drastically reduces. To verify the current MD results, the critical strain and stress values of pristine graphene reported by other researchers using different techniques are compared with our results, as summarized in Table 4.1. The comparison is found to be in good agreement with the published results (Ansari *et al.*, 2012; Lee *et al.*, 2008; Liu *et al.*, 2007).

Figure 4.10 represents the variation of stress and strain along the uniaxial direction of graphene containing different defect concentrations. Figure 4.10 depicts that the critical stress and critical strain decrease with increment in the concentration of defects. So, increasing the active sites by providing the defects can lead to a decrement in the strength of the graphene. So, we cannot exceed the defect concentration by a specific limit. We have plotted this graph by considering the different concentrations of monovacancy defect in the sheet ranging from 0.25, 0.50, 1, and 2% of defects in the graphene layer.

Table 4.2: Comparison of critical strain and stress of pristine graphene predicted by different methods

Method	Critical strain	Critical stress (GPa)	Ref.
Experimental	25%	130 ± 10	Lee <i>et al.</i>
<i>Ab initio</i>	19.4%	110	Liu <i>et al.</i>
MD simulations	23.3%	127	Ansari <i>et al.</i>
MD simulations	20%	134.83	Present

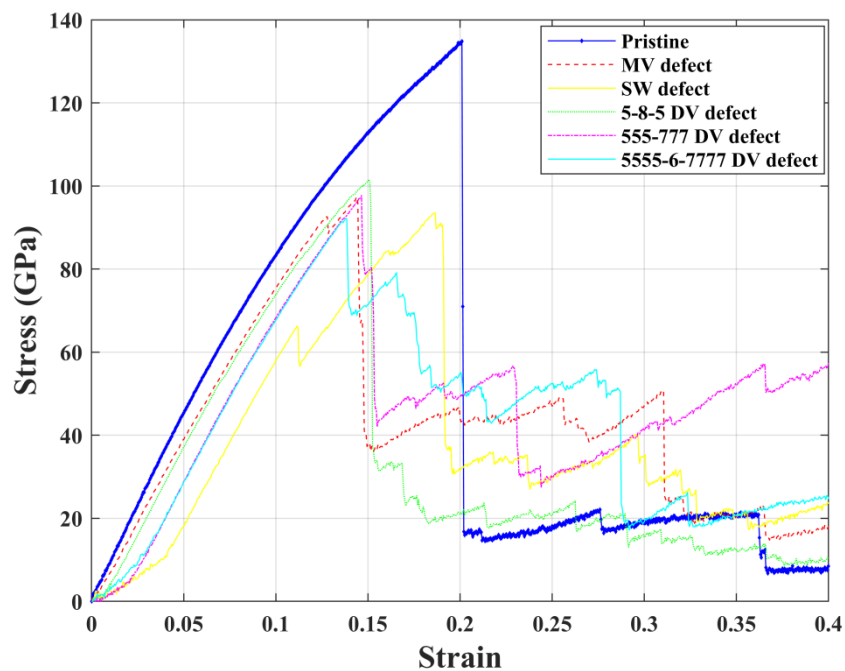


Fig. 4.9 Uniaxial tensile test in armchair direction of pristine and defected graphene.

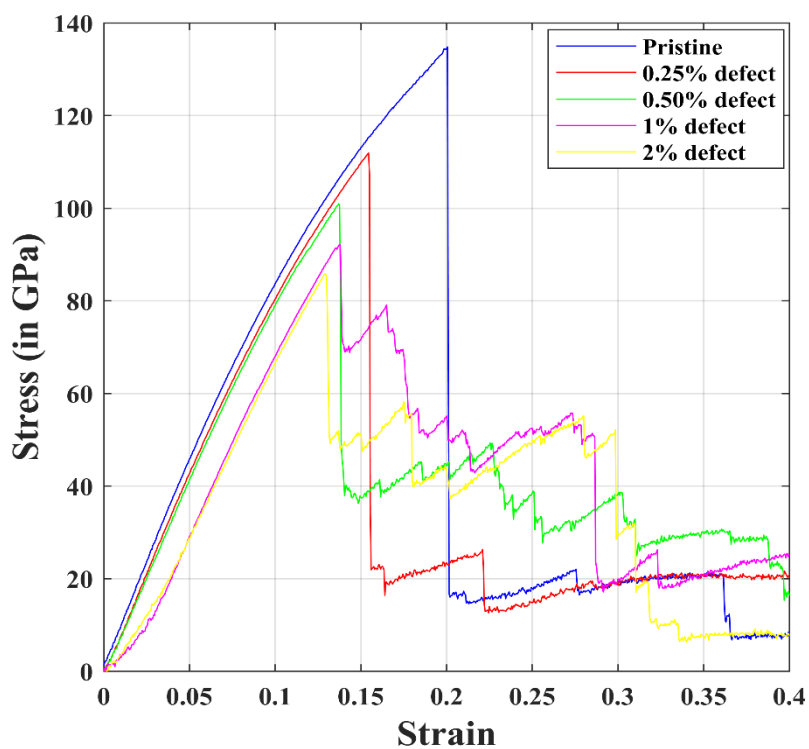


Fig. 4.10 Uniaxial tensile test of pristine graphene containing different concentration of defect

4.4 Conclusions

In this chapter, we have discussed the effect of different types of defects on the storage of hydrogen on graphene via MD simulations. The effect of defect concentration on the strength, critical stress and critical strain of graphene is also studied.

- Average adsorption energy calculation for the pristine sheet with varying pressure implies that at lower temperature or adsorption temperature (77 K) the magnitude is high as compared to the magnitude of energy at higher temperature or desorption temperature (300 K).
- Due to the higher magnitude of adsorption energy at lower temperatures, there is a strong binding of hydrogen with graphene sheets.
- As the pressure increases, the wt.% increases and saturate after the pressure of 50 bar, and the maximum holding capacity of hydrogen is achieved.
- The defected graphene sheets have more capacity to store the hydrogen as compared to the pristine sheets.
- The following wt.% of H₂ was found in the different cases: 9.3 wt.% in MV, 7.23 wt.% in SW, 8.763 wt.% in 5-8-5 DV, 8.17 wt.% 555-777, and 8.62 wt.% 5555-6-7777 DV at a 100 bar and 77 K; while 6.55 wt.% in pristine graphene at 100 bar and 77 K, respectively.
- The graphene layer with the MV defect can adsorb more H₂ molecules as compared to other types of defects.
- If defect concentration increases, the wt.% of H₂ in graphene increases, but at the same time, the strength analysis shows that the critical stress and critical strain decrease.

Chapter 5

Conclusions and future scope

In this chapter, major conclusions drawn from the current research work are highlighted. Moreover, the scope for further research on graphene for the application in energy storage is suggested.

5.1 Major conclusions

This thesis studies the graphene subjected to strain and its effect on the storage of hydrogen via MD simulations. We used the potential energy method to calculate the wt.% of hydrogen. We considered different types of defects in the graphene which occurs usually during synthesis and investigated their effect on the gravimetric density of hydrogen. The average adsorption energy calculations helped us to identify which type of defect possesses the maximum capacity to hold hydrogen.

The following main conclusions are drawn from the work carried out in this thesis:

- The potential energy distribution method provides good results compared to all other methods available in the literature.
- Graphene sheet subjected to the strain makes it reactive and found that the wt.% of hydrogen increases on the application of strain up to 10%.
- The system is very well equilibrating with a time step of 0.001 ps when running up to 1 ns.
- Average adsorption energy calculation for the pristine sheet with varying pressure implies that at lower temperature or adsorption temperature (77 K) the magnitude is high as compared to the magnitude of energy at higher temperature or desorption temperature (300 K).
- A higher magnitude of adsorption energy at lower temperatures indicates strong binding of hydrogen with the graphene.
- As the pressure increases, the wt.% of H₂ increases and saturate after pressure of 50 bar, and the maximum holding capacity of hydrogen can be achieved.

- The defected sheets have more capacity to store the hydrogen as compared to the pristine sheets.
- The following wt.% of H₂ was found in the different cases: 9.3 wt.% in MV, 7.23 wt.% in SW, 8.763 wt.% in 5-8-5 DV, 8.17 wt.% 555-777, and 8.62 wt.% 5555-6-7777 DV at a 100 bar and 77 K; while 6.55 wt.% in pristine graphene at 100 bar and 77 K, respectively.
- The graphene layer with the MV defect can adsorb more H₂ molecules compared to other types of defects.
- If defect concentration increases, the wt.% of H₂ in graphene increases, but at the same time, the strength analysis shows that the critical stress and critical strain decrease.

The present work offers a theoretical framework for predicting the hydrogen adsorption on the graphene layer, considering the strain and defects at 77 K and 300 K temperatures and different pressures.

5.2 Scope for future work

With the help of the first principle calculations, one can model 100 to 1000 atoms. But what about when we deal with a large number of atoms and molecules in the system? This problem can be solved with MD simulations, which deals with a huge number of atoms. MD simulation makes the calculation easy and creates a smooth pathway for the theoretical and practical studies with a specific set of approximations and reliable results. The current research is mainly done on the monolayer of graphene using the MD simulations. Some of the further research works that may be undertaken in line with the present work as follows:

- Using the outputs of the monolayer, one can study the hydrogen storage in or on bilayer and few-layer graphene via MD simulations.
- Study the hydrogen storage on graphene subjected to biaxial strain via MD simulations.
- Investigate the different types of possible defects in multilayer graphene.
- Unravelling the effect of the stacking of graphene (i.e., AA, AB etc.) on the storage of hydrogen.
- Establish an experimental setup for the storage of hydrogen on graphene at different temperature and pressure.

Appendix

Snapshots of MD simulations of pristine graphene subjected to tensile loading

The fracture of pristine graphene subjected to tensile loading along the armchair direction is shown in figure A1. Initially, the sheet is equilibrated at a temperature of 300 K and then subjected to tensile loading. A1 (a) shows the image of the sheet prior to fracture. Initiation of crack starts from the edges where stress concentration is more. A1 (b) shows the breaking of the bond or the initiation of the fracture. A1 (c) shows the propagation of fracture, the crack propagates along the perpendicular direction to the direction of loading, and A1 (d) shows the failure of the sheet at 20% of the strain.

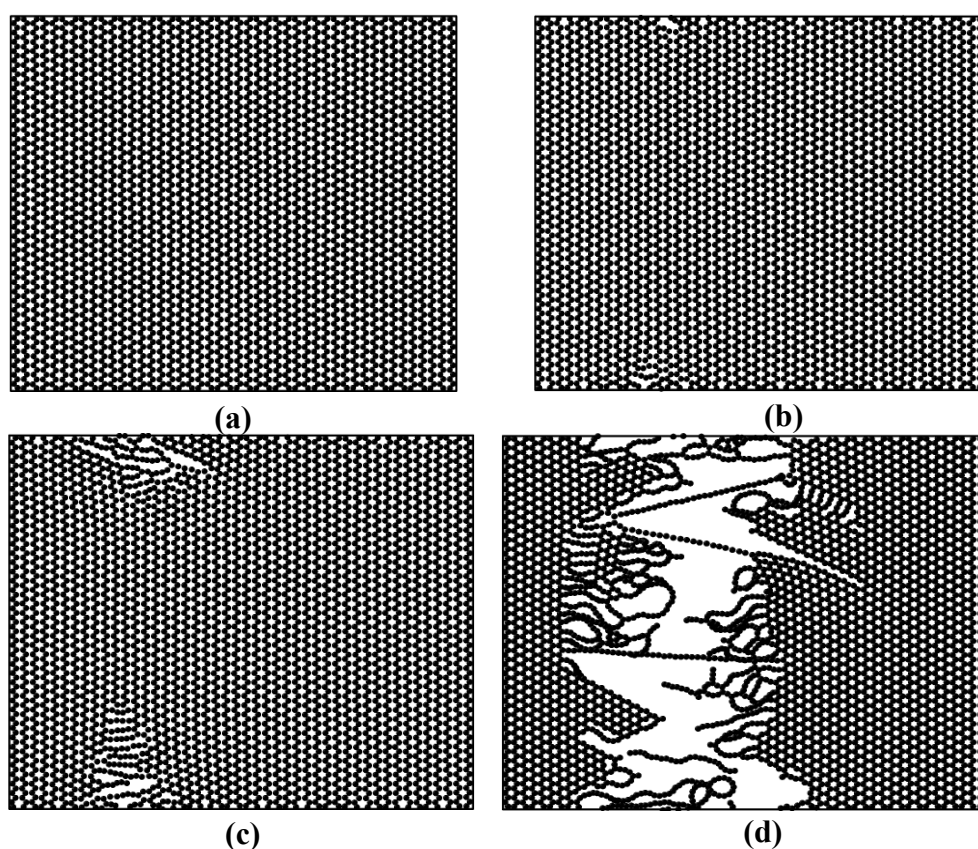


Fig. A1 (a) Pristine graphene prior to fracture, (b) initiation of bond breaking, (c) propagation of fracture, and (d) failure of sheet at 0.2 strain.

Snap shots of MD simulations of MV defected graphene subjected to tensile loading

The fracture of MV defected graphene subjected to tensile loading along the armchair direction is shown in figure A2. Initially, the sheet is equilibrated at a temperature of 300 K and then subjected to tensile loading. A2 (a) shows the image of sheet prior to fracture. A2 (b) shows the breaking of bond or the initiation of the fracture. A2 (c)

shows the propagation of fracture and A2(d) shows the failure of the sheet at 14.4% of the strain.

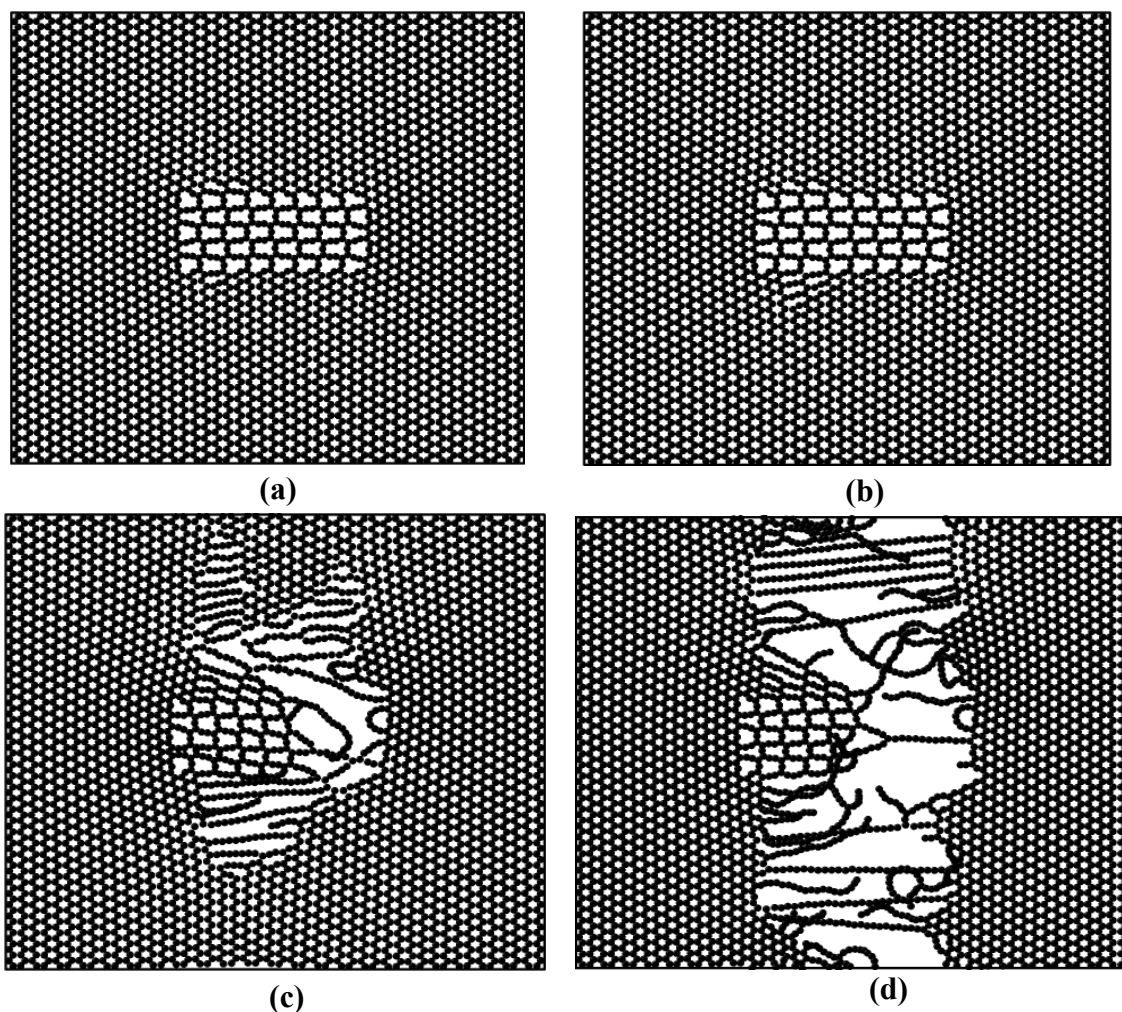


Fig. A2 (a) MV defected sheet prior to fracture, (b) initiation of bond breaking, (c) propagation of fracture, and (d) failure of MV defected sheet at 0.144 strain.

Snap shots of MD simulations of SW defected graphene subjected to tensile loading

The fracture of SW defected graphene subjected to tensile loading along the armchair direction is shown in Fig. A3. Initially, the sheet is equilibrated at a temperature of 300 K and then subjected to the tensile loading, A3(a) shows the image of sheet prior to fracture. A3(b) shows the breaking of bond or the initiation of the fracture. A3(c) shows the propagation of fracture and A3(d) shows the failure of sheet at 18.65% of the strain.

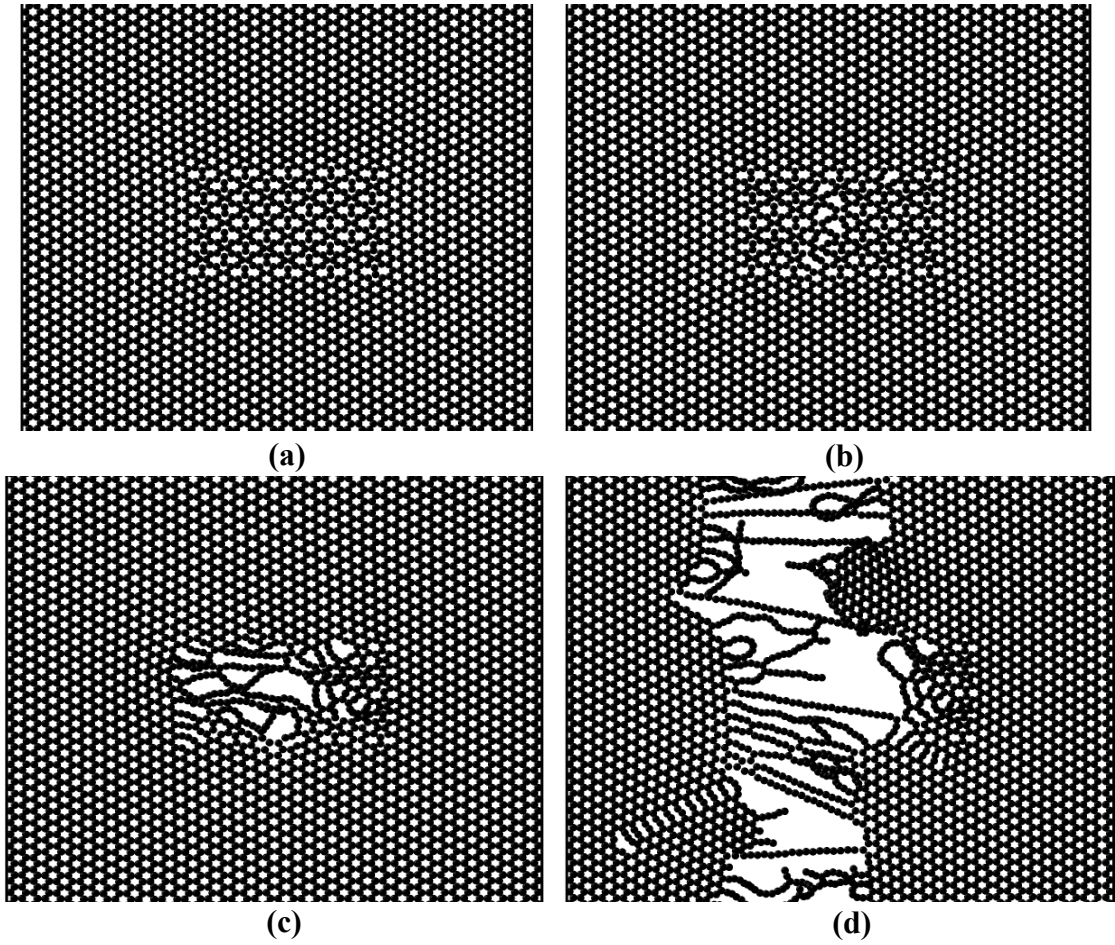


Fig. A3 (a) SW defected graphene prior to fracture, (b) initiation of bond breaking, (c) propagation of fracture, and (d) failure of SW defected sheet at 0.1865 strain.

Snap shots of MD simulations of 5-8-5 DV defected graphene subjected to tensile loading

The fracture of 5-8-5 DV defected graphene subjected to tensile loading along the armchair direction is shown in Fig. A4. Initially, the graphene is equilibrated at a temperature of 300 K and then subjected to the tensile loading. A4(a) shows the image of graphene prior to fracture. A4(b) shows the breaking of bond or the initiation of the fracture. A4(c) shows the propagation of fracture and A4(d) shows the failure of the sheet at 18.65% of the strain.

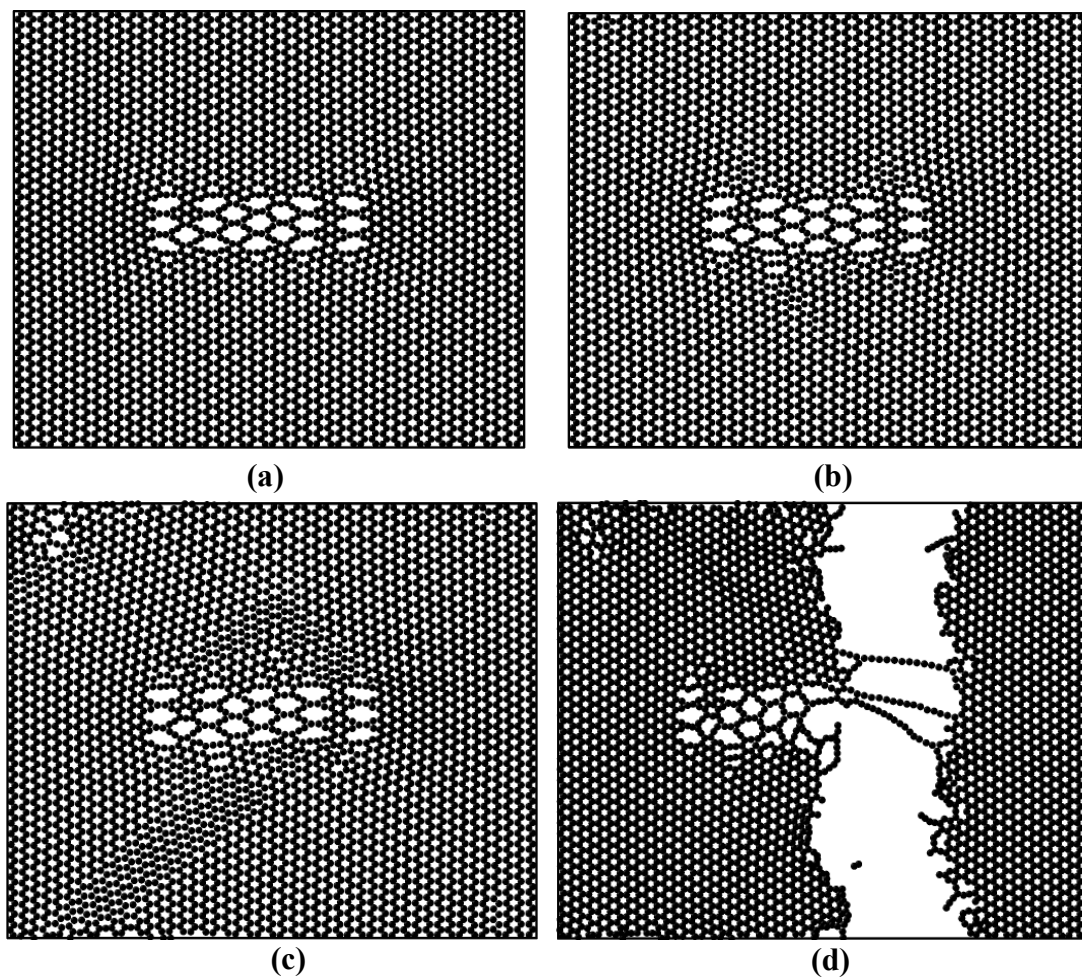


Fig. A4 (a) 5-8-5 DV defected sheet prior to fracture, (b) initiation of bond breaking, (c) propagation of fracture, and (d) failure of 5-8-5 DV defected sheet at 0.1505 strain.

Snap shots of MD simulations of 555-777 DV defected graphene subjected to tensile loading

The fracture of 555-777 DV defected graphene subjected to tensile loading along the armchair direction is shown in Fig. A5. Initially, the sheet is equilibrated at a temperature of 300 K and then subjected to the tensile loading. A5(a) shows the image of sheet prior to fracture. A5(b) shows the breaking of bond or the initiation of the fracture. A5(c) shows the propagation of fracture and A5(d) shows the failure of the sheet at 14.65% of the strain.

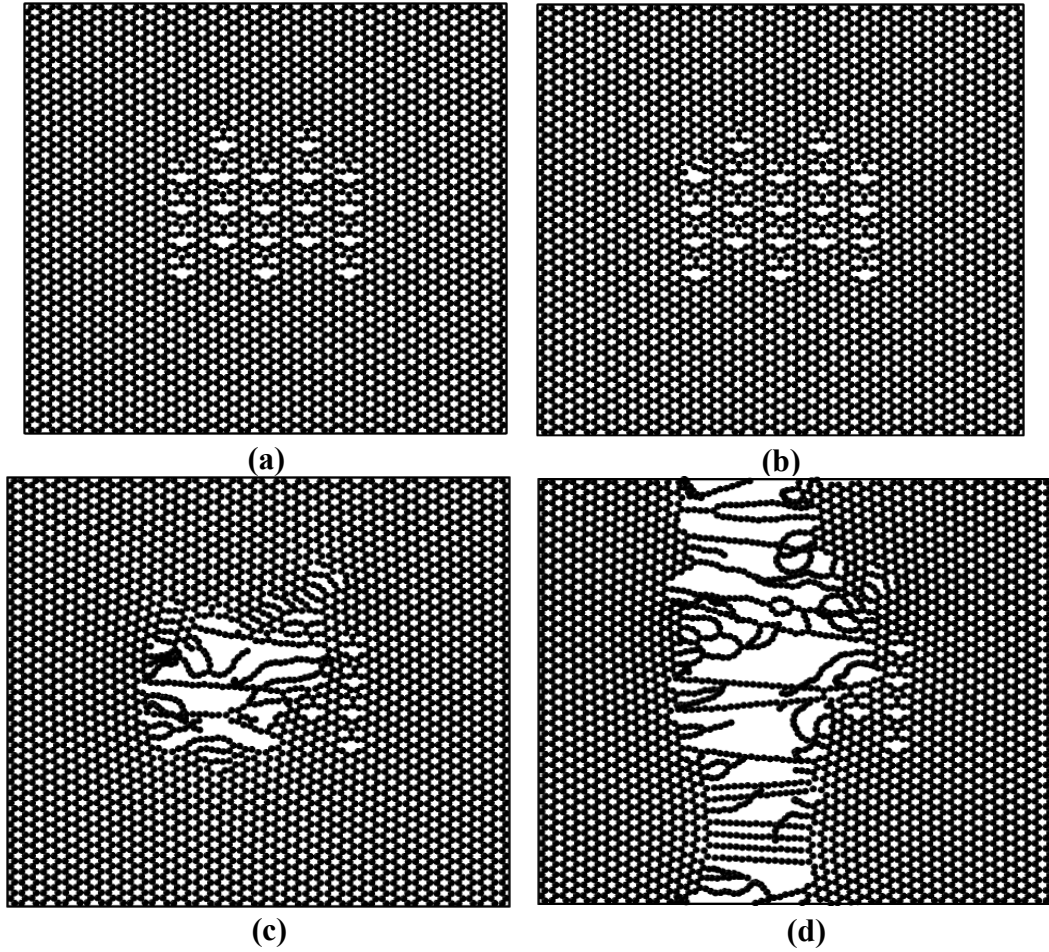


Fig. A5 (a) 555-777 DV defected graphene prior to fracture, (b) initiation of bond breaking, (c) propagation of fracture, and (d) failure of 555-777 DV defected sheet at 0.1465 strain.

Snap shots of MD simulations of 5555-6-7777 DV defected sheet subjected to tensile loading

The fracture of 5555-6-7777 DV defected graphene subjected to tensile loading along the armchair direction is shown in Fig. A6. Initially, the sheet is equilibrated at a temperature of 300 K and then subjected to the tensile loading. A6 (a) shows the image of sheet prior to fracture. A6 (b) shows the breaking of bond or the initiation of the fracture. A6 (c) shows the propagation of fracture and A6 (d) shows the failure of the sheet at 13.80% of the strain.

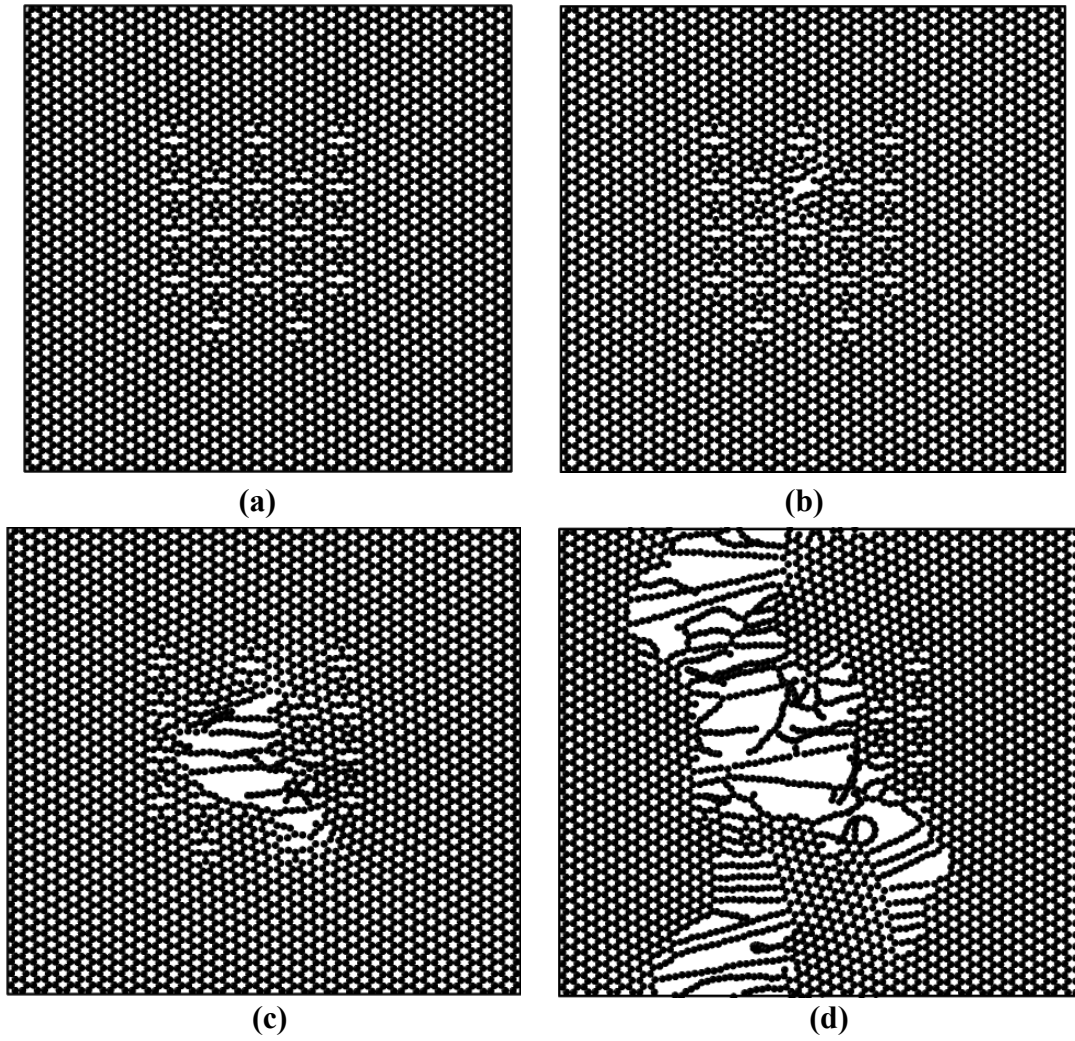


Fig. A6 (a) 5555-6-7777 DV defected sheet prior to fracture, (b) initiation of bond breaking, (c) propagation of fracture, and (d) failure of 5555-6-7777 DV defected sheet at 0.138 strain.

Table A1. The critical stress and critical strain of the pristine and defected graphene sheets

S. No.	Sheet	Critical Stress (GPa)	Critical Strain (in %)
1	Pristine	134.82	20
2	MV defected	97.384	14.4
3	SW defected	93.50	18.65
4	5-8-5 DV defected	101.561	15.05
5	555-777 DV defected	97.716	14.65
6	5555-6-7777 DV defected	92.179	13.8

Correlation of strain on adsorption of hydrogen over graphene

Figure A7 shows the correlation of strain on the adsorption of hydrogen over graphene. As time increases, the strain increases, and the hydrogen molecules form a layer-like structure around the sheet. The thickness of such adsorbed hydrogen layer increases with an increase in strain. Figure A7 (a) represents the sheet with zero strain, Fig. A7 (b) represents the sheet having a 0.025 (2.5%) of strain and Fig. A7 (c) represents the sheet with 0.05 (5%) strain. Then, the system was equilibrated, and we calculated wt.% of hydrogen as mentioned in section 2.4 of the thesis.

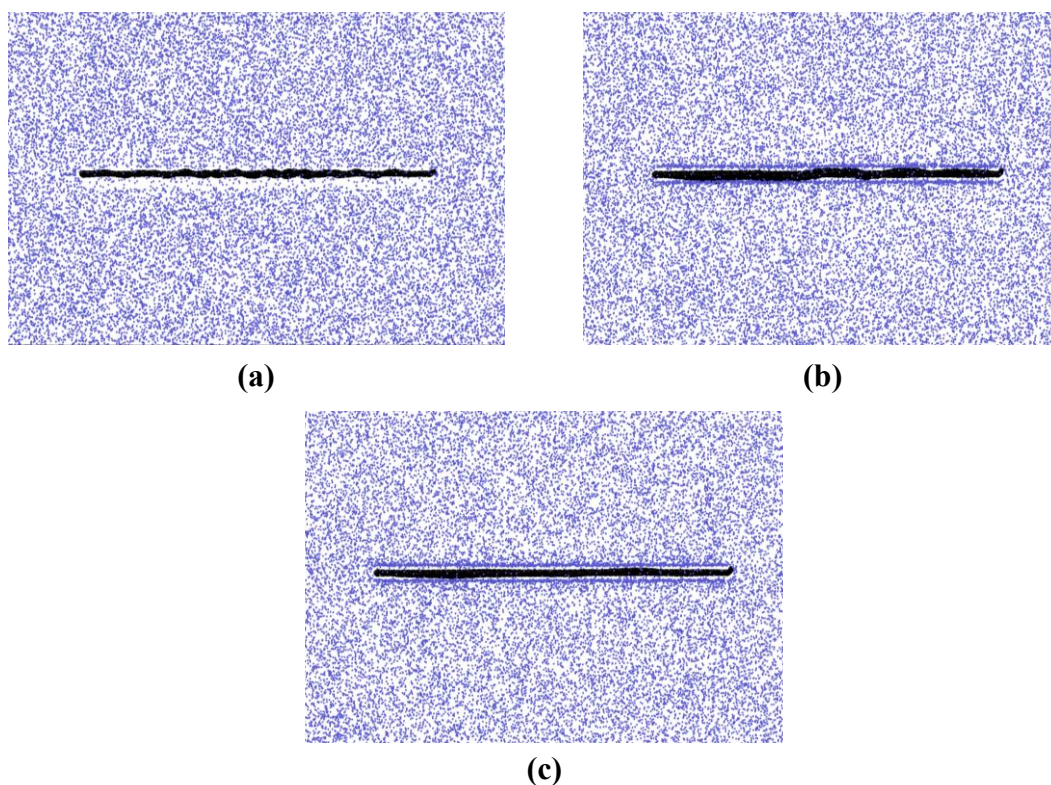


Fig. A7 represents the graphene sheet with (a) zero strain, (b) with 0.025 strain, and (c) with 0.05 strain at 77 K temperature and 10 bar pressure

References

Allen, M.P. (2004). Introduction to molecular dynamics simulation. *Comput. Soft Matter From Synth, Polym. to Proteins. Lecture Notes.* 23, pp.1–28.

Alian, A.R., Meguid, S.A. and Kundalwal, S.I. (2017) Unraveling the influence of grain boundaries on the mechanical properties of polycrystalline carbon nanotubes. *Carbon* 125:180–188. (DOI: 10.1016/j.carbon.2017.09.056)

Ao, Z., Dou, S., Xu, Z., Jiang, Q. and Wang, G. (2014) Hydrogen storage in porous graphene with Al decoration. *International Journal of Hydrogen Energy* 39:(28)16244–16251. (DOI: 10.1016/j.ijhydene.2014.01.044)

Ansari, R., Ajori, S. and Motevalli, B. (2012) Mechanical properties of defective single-layered graphene sheets via molecular dynamics simulation. *Superlattices and Microstructures* 51:(2)274–289. (DOI: 10.1016/j.spmi.2011.11.019)

Arachchige, N. (2012) Molecular Dynamics Study of Effects of geometric defects on the mechanical properties of graphene, pp.82–101. (DOI: 10.14288/1.0072708)

Ariharan, A., Viswanathan, B. and Nandhakumar V. (2017) Nitrogen doped graphene as potential material for hydrogen storage. *Graphene* 6:(2)41–60. (DOI: 10.4236/graphene.2017.62004)

Balat, M. (2009) Possible methods for hydrogen production, *Energy Sources, Part A Recover. Util. Environ. Eff.* 31, 39–50. (DOI: 10.1080/15567030701468068)

Banhart, F., Kotakoski, J. and Krasheninnikov, A.V. (2011) Structural defects in graphene. *ACS Nano.* (DOI: 10.1021/nn102598m)

Bartels, J.R., Pate, M.B. and Olson, N.K. (2010) An economic survey of hydrogen production from conventional and alternative energy sources. *International Journal of Hydrogen Energy* 35, 8371–8384. (DOI: 10.1016/j.ijhydene.2010.04.035)

Barrett, S. (2005) Progress in the European hydrogen & fuel cell technology platform. *Fuel Cells Bulletin* (4)pp. 12–17. (DOI: 10.1016/S1464-2859(05)00591-2)

Bénard, P. and Chahine, R. (2001) Modeling of adsorption storage of hydrogen on activated carbons. *International Journal of Non-Linear Mechanics* 36:(8)849–855. (DOI: 10.1016/S0360-3199(01)00018-0)

Berendsen, H.J.C., Postma, J.P.M., Van Gunsteren, W.F., Dinola, A., and Haak, J.R. (1984). Molecular dynamics with coupling to an external bath. *J. Chem. Phys.* 81, pp.3684–3690. (DOI: 10.1063/1.448118)

Bhuyan, M.S.A., Uddin, M.N., Islam, M.M., Bipasha, F.A. and Hossain, S.S. (2016) Synthesis of graphene. *Int. Nano Lett.* 6, 65–83. (DOI:10.1007/s40089-015-0176-1)

Bičáková, O. and Straka, P. (2012) Production of hydrogen from renewable resources and its effectiveness. *Int. J. Hydrogen Energy.* (DOI: 10.1016/j.ijhydene.2012.05.047)

Blanco-Rey, M., Juaristi, J.I., Alducin, M., López, M.J. and Alonso, J.A. (2016) Is spillover relevant for hydrogen adsorption and storage in porous carbons doped with palladium nanoparticles? *The Journal of Physical Chemistry C* 120:(31)17357-17364. (DOI: 10.1021/acs.jpcc.6b04006)

Borodin, V.A., Vehviläinen, T.T., Ganchenkova, M.G. and Nieminen, R.M. (2011) Hydrogen transport on graphene: Competition of mobility and desorption. *Physical Review B* 84:(7)075486. (DOI: 10.1103/PhysRevB.84.075486)

BP Statistical Review of World Energy (2018) Statistical Review of World Energy June 2018. BP Statistical Review of World Energy.

Chae, H.K., Siberio-Pérez, D.Y., Kim, J., Go, Y.B., Eddaoudi, M., Matzger, A.J., O’Keeffe, M. and Yaghi, O.M. (2004) A route to high surface area, porosity, and inclusion of large molecules in crystals. *Nature* 427:(6974)523–527. (DOI: 10.1038/nature02311)

Chang, E. C. (2017) Robust and optimal technical method with application to hydrogen fuel cell systems. *International Journal of Hydrogen Energy* 42(40), pp. 25326–25333. (DOI: 10.1016/j.ijhydene.2017.08.119)

Choi, W., Lahiri, I., Seelaboyina, R. and Kang, Y.S. (2010) Synthesis of graphene and its applications: A review. *Critical Reviews in Solid and Materials Sciences* 35:(1)52-71. (DOI: 10.1080/10408430903505036)

Ci, L., Zhu, H., Wei, B., Xu, C. and Wu, D. (2002) Annealing amorphous carbon nanotubes for their application in hydrogen storage. *Appl. Surf. Sci.* 205, 39–43. (DOI: 10.1016/S0169-4332(02)00897-8)

Cooper, V.R., Ihm, Y. and Morris, J.R. (2012) Hydrogen adsorption at the graphene surface: A vdW-DF perspective. *Phys. Procedia* 34,34-38. (DOI: 10.1016/j.phpro.2012.05.005)

Costanzo, F., Silvestrelli, P.L. and Ancilotto, F. (2012) Physisorption, diffusion, and chemisorption pathways of H₂ molecule on graphene and on (2,2) carbon nanotube by first principles calculations. *Journal of Chemical Theory and Computation* 8:(4)1288–1294. (DOI: 10.1021/ct300143a)

Dante, R.C., Güereca, L.P., Neri, L., Escamilla, J.L., Aquino, L. and Celis, J. (2002) Life cycle analysis of hydrogen fuel: A methodology for a strategic approach of decision making. *International Journal of Hydrogen Energy* 27:(2)131–133. (DOI: 10.1016/S0360-3199(01)00098-2)

Das, T.K., Banerjee, S., Sharma, P., Sudarsan, V. and Sastry, P.U. (2018) Nitrogen

doped porous carbon derived from EDTA: Effect of pores on hydrogen storage properties. *Int. J. Hydrogen Energy* 43, 8385–8394. (DOI: 10.1016/j.ijhydene.2018.03.081)

Deng, S., Sumant, A.V. and Berry, V. (2018) Strain engineering in two-dimensional nanomaterials beyond graphene. *Nano Today* 22:14–35. (DOI: 10.1016/j.nantod.2018.07.001)

Denis, P.A. and Iribarne, F. (2013) A Comparative Study of Defect Reactivity in Graphene A Comparative Study of Defect Reactivity in Graphene. (DOI: 10.1021/jp4061945)

Deretzis, I., Piccitto, G. and Magna, A.La. (2012) Electronic transport signatures of common defects in irradiated graphene-based systems. *Nuclear Instruments and Methods in Physics Research, Section B: Beam Interactions with Materials and Atoms* (DOI: 10.1016/j.nimb.2011.08.052)

Dincer, I. (2012) Green methods for hydrogen production. *Int. J. Hydrogen Energy* 37, 1954–1971. (DOI: 10.1016/j.ijhydene.2011.03.173)

Durbin, D.J. (2013) Review of hydrogen storage techniques for on board vehicle applications 1–23. (DOI: 10.1016/j.ijhydene.2013.07.058)

Dutta, S. (2014) A review on production, storage of hydrogen and its utilization as an energy resource. *J. Ind. Eng. Chem.* 20, 1148–1156. (DOI: 10.1016/j.jiec.2013.07.037)

Eberle, U., Felderhoff, M. and Schüth, F. (2009) Chemical and physical solutions for hydrogen storage. *Angew. Chemie - Int. Ed.* 48, 6608–6630. (DOI: 10.1002/anie.200806293)

Evans, D.J., Holian, and B.L. (1985). The Nose-Hoover thermostat. *J. Chem. Phys.* 83, pp.4069. (DOI: 10.1063/1.449071)

Georgakis, M., Stavropoulos, G. and Sakellaropoulos, G.P. (2014) Alteration of graphene based slit pores and the effect on hydrogen molecular adsorption: A simulation study. *Microporous and Mesoporous Materials* 191:67-73. (DOI: 10.1016/j.micromeso.2014.02.042)

Hockney, R.W. (1970). The potential calculation and some applications, in: *Methods in Computational Physics*, 9, pp.136.

Houf, W. G., Evans, G.H., Ekoto, I.W., Merilo, E.G. and Groethe, M.A. (2013) Hydrogen fuel-cell forklift vehicle releases in enclosed spaces. *International Journal of Hydrogen Energy* 38(19), pp. 8179–8189. (DOI: 10.1016/j.ijhydene.2012.05.115)

Hünenberger, P.H. (2005). Thermostat algorithms for molecular dynamics simulations. *Adv. Polym. Sci.* 173, pp.105–149. (DOI: 10.1007/b99427)

Hussain, T., De Sarkar, A. and Ahuja, R. (2012) Strain induced lithium functionalized graphene as a high capacity hydrogen storage material. *Appl. Phys. Lett.* 101. (DOI: 10.1063/1.4751249)

Indian country status report on hydrogen and fuel cell by DST (2020) India country status report on hydrogen fuel cells Department of Science and Technology New Delhi.

Iniguez, J. (2008) Modelling of carbon-based materials for hydrogen storage, *Solid-State Hydrogen Storage: Materials and Chemistry* 205-220. (DOI: 10.1533/9781845694944.2.205)

Kanitkar, T., Banerjee, R., and Jayaraman, T. (2018) An integrated modeling framework for energy economy and emissions modeling: A case for India. *Energy*. (DOI: 10.1016/j.energy.2018.11.025)

Katin, K.P., Prudkovskiy, V.S. and Maslov, M.M., (2017) Chemisorption of hydrogen atoms and hydroxyl groups on stretched graphene: A coupled QM/QM study. *Physics Letters A*, 381(33), pp.2686-2690. (DOI: 10.1016/j.physleta.2017.06.017)

Kim, D., Lee, S., Hwang, Y., Yun, K.H. and Chung YC (2014) Hydrogen storage in Li dispersed graphene with Stone-Wales defects: A first-principles study. *International Journal of Hydrogen Energy* 39:(25)13189–13194. (DOI: 10.1016/j.ijhydene.2014.06.163)

Kothari, R., Buddhi, D. and Sawhney, R.L. (2008) Comparison of environmental and economic aspects of various hydrogen production methods. *Renew. Sustain. Energy Rev.* (DOI:10.1016/j.rser.2006.07.012)

Kothari, R., Kundalwal, S.I. and Sahu, S.K. (2018) Transversely isotropic thermal properties of carbon nanotubes containing vacancies. *Acta Mechanica* 229:(7)2787–2800. (DOI: 10.1007/s00707-018-2145-z)

Kundalwal, S.I., Choyal, V. (2018). Transversely isotropic elastic properties of carbon nanotubes containing vacancy defects using MD. *Acta Mech.* 229, pp.2571–2584. (DOI: 10.1007/s00707-018-2123-5)

Lee, C., Wei, X., Kysar, J.W. and Hone, J. (2008) Measurement of the elastic properties and intrinsic strength of monolayer graphene. *Science* (80-.). 321, 385–388. (DOI: 10.1126/science.1157996)

Liao, J.H., Zhao, Y.J. and Yang, X.B. (2015) Controllable hydrogen adsorption and desorption by strain modulation on Ti decorated defective graphene. *International Journal of Hydrogen Energy* 40:(36)12063–12071. (DOI: 10.1016/j.ijhydene.2015.07.083)

Liu, F., Ming, P. and Li, J. (2007) Ab initio calculation of ideal strength and phonon instability of graphene under tension. *Physical Review B - Condensed Matter and Materials Physics* 76:(6)1–7. (DOI: 10.1103/PhysRevB.76.064120)

Luhadiya, N., Kundalwal, S.I., Sahu, S.K. (2021) Investigation of hydrogen adsorption behavior of graphene under varied conditions using a novel energy-centered method. *Carbon Letters*. (DOI: 10.1007/s42823-021-00236-3)

Ma, L.P., Wu, Z.S., Li, J., Wu, E.D., Ren, W.C. and Cheng, H.M. (2009) Hydrogen adsorption behavior of graphene above critical temperature. *International Journal of Hydrogen Energy*, 34(5)2329-2322. (DOI: 10.1016/j.ijhydene.2008.12.079)

Martyna, G.J., Tobias, D.J., and Klein, M.L. (1994). Constant pressure molecular dynamics algorithms. *J. Chem. Phys.* 101, pp.4177. (DOI: 10.1063/1.467468)

Nagar, R., Vinayan, B.P., Samantaray, S.S. and Ramaprabhu S. (2017) Recent advances in hydrogen storage using catalytically and chemically modified graphene nanocomposites. *Journal of Materials Chemistry A* 5:(44)22897–22912. (DOI: 10.1039/c7ta05068b)

Novoselov, K.S., Geim, A.K., Morozov, S.V., Jiang, D., Zhang, Y., Dubonos, S.V., Grigorieva, I.V. and Firsov, A.A. (2004) Electric field in atomically thin carbon films. *Science*. (DOI: 10.1126/science.1102896)

Park, H.L., Yi, S.C. and Chung, Y.C. (2010) Hydrogen adsorption on Li metal in boron-substituted graphene: An ab initio approach. *International Journal of Hydrogen Energy* 35:(8)3583–3587. (DOI: 10.1016/j.ijhydene.2010.01.073)

Perreault, F., Fonseca De Faria, A. and Elimelech, M. (2015) Environmental applications of graphene- based nanomaterials. *Chem. Soc. Rev.* 44, 5861–5896. (DOI: 10.1039/c5cs00021a)

Rapaport, D. C. (2004) *The Art of Molecular Dynamics Simulation*, The Art of Molecular Dynamics Simulation. (DOI: 10.1017/cbo9780511816581)

Rapaport, D.C. (2011). Basic molecular dynamics, in: *The Art of Molecular Dynamics Simulation*. pp.11–43. (DOI: 10.1017/cbo9780511816581.005)

Rao, CNR., Sood, A.K., Subrahmanyam, K.S. and Govindaraj, A. (2009) Graphene: The new two- dimensional nanomaterial, *Angewandte Chemie - International Edition* 48:(42)7752–7777. (DOI: 10.1002/anie.200901678)

Rozada, R., Paredes, J.I., López, M.J., Villar-Rodil, S., Cabria, I., Alonso, J.A., Martínez-Alonso, A. and Tascón, J.M. (2015) From graphene oxide to pristine graphene: revealing the inner workings of the full structural restoration, *Nanoscale* 7:(6)2374-2390. (DOI: 10.1039/C4NR05816J)

Schlapbach, L. (2009) Hydrogen-fuelled vehicles. *Nature* 460(7257), pp. 809–811. (DOI: 10.1038/460809a)

Seenithurai, S., Pandyan, R.K., Kumar, S.V., Saranya, C. and Mahendran, M. (2014) Li-decorated double vacancy graphene for hydrogen storage application: A first principles study. *International Journal of Hydrogen Energy* 39:(21)11016–11026. (DOI: 10.1016/j.ijhydene.2014.05.068)

Sen, D., Thapa, R. and Chattopadhyay, K.K. (2013) Small Pd cluster adsorbed double vacancy defect graphene sheet for hydrogen storage: A first-principles study.

International Journal of Hydrogen Energy 38:(7)3041–3049. (DOI: 10.1016/j.ijhydene.2012.12.113)

Shen, S. and Hu, S. (2010). A theory of flexoelectricity with surface effect for elastic dielectrics. *J. Mech. Phys. Solids*. 58, pp.665–677. (DOI: 10.1016/j.jmps.2010.03.001)

Shiraz, H.G. and Tavakoli, O. (2017) Investigation of graphene-based systems for hydrogen storage. *Renewable and Sustainable Energy Reviews* 74:104-109. (DOI: 10.1016/j.rser.2017.02.052)

Simon, J.M., Haas, O.E. and Kjelstrup, S. (2010) Adsorption and desorption of H₂ on graphite by molecular dynamics simulations. *The Journal of Physical Chemistry C* 114:(22)10212-10220. (DOI: 10.1021/jp1011022)

Singh, D.K., Maiti, S.K., Bhandakkar, T.K. and Raman, R.K.S. (2018) Cohesive zone based axisymmetric modelling of hydrogen-assisted cracking in a circumferentially notched tensile specimen. *Int. J. Hydrogen Energy* 43, 12530–12542. (DOI: 10.1016/j.ijhydene.2018.04.188)

Srinivas, G., Zhu, Y., Piner, R., Skipper, N., Ellerby, M., Ruoff, R. (2010) Synthesis of graphene-like nanosheets and their hydrogen adsorption capacity. *Carbon* 48:(3)630–635. (DOI: 10.1016/j.carbon.2009.10.003)

Ströbel, R., Garche, J., Moseley, P.T., Jörisen, L. and Wolf, G. (2006) Hydrogen storage by carbon materials. *Journal of Power Sources* 159:(2)781–801. (DOI: 10.1016/j.jpowsour.2006.03.047)

Stuart, S.J., Tutein, A.B. and Harrison, J.A. (2000) A reactive potential for hydrocarbons with intermolecular interactions. *Journal of Chemical Physics* 112:(14)6472–6486. (DOI: 10.1063/1.481208)

Stukowski, A. (2010). Visualization and analysis of atomistic simulation data with OVITO-the Open Visualization Tool. *Model. Simul. Mater. Sci. Eng.* 18, pp.015012. (DOI: 10.1088/0965-0393/18/1/015012)

Sunnardianto, G.K., Bokas, G., Hussein, A., Walters, C., Moulto, O.A. and Dey, P. (2021) Efficient hydrogen storage in defective graphene and its mechanical stability: A combined density functional theory and molecular dynamics simulation study. *International Journal of Hydrogen Energy* 46:(7)5485-5494. (DOI: 10.1016/j.ijhydene.2020.11.068)

Surya, V.J., Iyakutti, K., Mizuseki, H. and Kawazoe, Y. (2012) Modification of graphene as active hydrogen storage medium by strain engineering. *Computational Materials Science* 65:144–148. (DOI: 10.1016/j.commatsci.2012.07.016)

Swope, W.C., Andersen, H.C., Berens, P.H. and Wilson, K.R. (1982). A computer simulation method for the calculation of equilibrium constants for the formation of physical clusters of molecules: Application to small water clusters. *J. Chem. Phys.* 76, pp.637–649. (DOI: 10.1063/1.442716)

Tiwari, S. and Sharma, P. (2019) Simulations of hydrogen-storage system integrated with sensible storage system. *Nanomater. Energy* 8, 33–41. (DOI: 10.1680/jnaen.18.00016)

Wang, Y., Liu, J., Wang, K., Chen, T., Tan, X. and Li, C.M. (2011) Hydrogen storage in Ni-B nanoalloy-doped 2D graphene. *International Journal of Hydrogen Energy* 36:(20)12950–12954. (DOI: 10.1016/j.ijhydene.2011.07.034)

Wu, C.D., Fang, T.H. and Lo, J.Y. (2012) Effects of pressure, temperature, and geometric structure of pillared graphene on hydrogen storage capacity. *International Journal of Hydrogen Energy*, 37:(19)14211-14216. (DOI: 10.1016/j.ijhydene.2012.07.040)

Xue, K. and Xu, Z. (2010) Strain effects on basal-plane hydrogenation of graphene: A first-principles study. *Applied Physics Letters* 96:(6)063103. (DOI: 10.1063/1.3298552)

Yadav, S., Zhu, Z. and Singh, C.V. (2014) Defect engineering of graphene for effective hydrogen storage. *International Journal of Hydrogen Energy* 39:(10)4981–4995. (DOI: 10.1016/j.ijhydene.2014.01.051)

Zheng, Q., Ji, X., Gao, S. and Wang, X. (2013) Analysis of adsorption equilibrium of hydrogen on graphene sheets. *International Journal of Hydrogen Energy* 38:(25)10896-10902. (DOI: 10.1016/j.ijhydene.2013.01.098)

Zhou, L. (2005) Progress and problems in hydrogen storage methods. *Renew. Sustain. Energy Rev.* 9, 395–408. (DOI: 10.1016/j.rser.2004.05.005)

Zhou, M., Lu, Y., Zhang, C., and Feng, Y.P. (2010) Strain effects on hydrogen storage capability of metal-decorated graphene: A first-principles study. *Applied Physics Letters* 97:(10). (DOI: 10.1063/1.3486682)

List of publication

The following paper is published from the research work carried out in the MS(R).

Journal Publication from the thesis

Deepak Kag, Nitin Luhadiya, Nagesh D. Patil, S.I. Kundalwal. Strain and defect engineering of graphene for hydrogen storage via atomistic modelling. International Journal of Hydrogen Energy 2021;46(43):22599-22610. (DOI: 10.1016/j.ijhydene.2021.04.098) (I.F.: 5.816)